Received: 15 July 2021 | Accepted: 4 September 2021

DOI: 10.1002/ctpp.202100126

REVIEW ARTICLE

Contributions to Plasma Physics

Physical aspects of dust–plasma interactions

M.Y. Pustylnik[1] | **A.A. Pikalev**[1] | **A.V. Zobnin**[2] | **I.L. Semenov**[3] | **H.M. Thomas**[1] | **O.F. Petrov**[2]

[1]Forschungsgruppe Komplexe Plasmen, Institut für Materialphysik im Weltraum, Deutsches Zentrum für Luft- und Raumfahrt, Weßling, Germany

[2]Dusty Plasmas Department, Joint Institute for High Temperatures, Russian Academy of Sciences, Moscow, Russia

[3]Plasma Life Science Department, Leibniz Institute for Plasma Science and Technology, Greifswald, Germany

Correspondence
M.Y. Pustylnik, Institut für Materialphysik im Weltraum, Deutsches Zentrum für Luft- und Raumfahrt, Münchener Straße 20, 82234 Weßling, Germany.
Email: mikhail.pustylnik@dlr.de

Funding information
Bayerisches Staatsministerium für Wirtschaft, Infrastruktur, Verkehr und Technologie; Deutscher Akademischer Austauschdienst; Deutsches Zentrum für Luft- und Raumfahrt, Grant/Award Number: 50WM1441; Ministry of Science and Higher Education of the Russian Federation, Grant/Award Number: 075-00460-21-00

Abstract

Low-pressure gas discharge plasmas are known to be strongly affected by the presence of small dust particles. This issue plays a role in the investigations of dust particle-forming plasmas, where the dust-induced instabilities may affect the properties of synthesized dust particles. Also, gas discharges with large amounts of microparticles are used in microgravity experiments, where strongly coupled subsystems of charged microparticles represent particle-resolved models of liquids and solids. In this field, deep understanding of dust–plasma interactions is required to construct the discharge configurations which would be able to model the desired generic condensed matter physics as well as, in the interpretation of experiments, to distinguish the plasma phenomena from the generic condensed matter physics phenomena. In this review, we address only physical aspects of dust–plasma interactions, that is, we always imply constant chemical composition of the plasma as well as constant size of the dust particles. We also restrict the review to two discharge types: dc discharge and capacitively coupled rf discharge. We describe the experimental methods used in the investigations of dust–plasma interactions and show the approaches to numerical modelling of the gas discharge plasmas with large amounts of dust. Starting from the basic physical principles governing the dust–plasma interactions, we discuss the state-of-the-art understanding of such complicated, discharge-type-specific phenomena as dust-induced stratification and transverse instability in a dc discharge or void formation and heartbeat instability in an rf discharge.

KEYWORDS

complex plasmas, dc discharges, dusty plasmas, rf discharges

1 | INTRODUCTION

In the last decades, several enabling technologies ranging from manufacturing of modern microelectronic devices to electric propulsion in space were brought to life with the help of low-temperature plasmas.[1] Practically, every sector of the society has benefited and will continue benefiting from the improvements in the understanding of fundamental processes in low-temperature plasmas. Dusty (or complex) plasmas represent a class of low-temperature and (usually also) low-pressure plasmas containing along with free electrons, ions, neutral molecules, radiation and also the nanometre- or

micrometre-sized solid particles. They can be found in nature in the form of planetary rings, comet tails, or noctilucent clouds, as well as in industrial plasma reactors.[2–4]

Dust particles immersed in plasmas represent a new plasma component with unusual properties.[2,3,5–7] They (a) absorb the fluxes of plasma species on their surfaces, (b) acquire relatively large negative charges that are non-negligible in the net charge balance of the plasmas and are self-consistently coupled to the local plasma conditions, (c) exhibit relatively slow dynamics due to the low charge-to-mass ratio, and (d) become sensitive to fluxes and temperature gradients in charged as well as in the neutral components of the plasma. Therefore, dusty plasmas cannot be treated as ensembles of dust particles immersed in dust-free plasmas, and dust–plasma interactions need to be taken into account. "Tuning of plasma–dust grain interactions for precision control of trajectories and growth of nano- and micro-particles" is stated as one of the future challenges for the field dusty plasmas in the decadal assessment of plasma science performed by the US National Academies of Science, Engineering and Medicine.[1] Such a vision is driven mainly by two emerging research directions.

First of all, the possibilities of using plasmas for production of nanocrystals are being actively investigated.[4] Semiconductor nanocrystals have led to promising advancements in many fields. Among those are, for example, solar cells, quantum dot light-emitting diodes, bioimaging, or nanocomposite materials.[8] Plasma synthesis of dust particles exhibits a number of advantages if compared with wet chemistry or other gas-phase synthesis approaches. It requires neither solvents nor ligands, allows to work with high melting point materials, prevents the dust particles from coagulation by means of charging, etc. Recently, a great progress has been achieved in this field. Elemental, alloy, and doped group IV semiconductor nanocrystals, compound semiconductor nanocrystals, and metal dust particles can be presently synthesized using plasmas. Further advances in this field which would result in plasma synthesis of heterostructures or multicomponent materials are hardly possible without deep understanding of dust–plasma interactions.

The other field involving dusty plasmas is the basic interdisciplinary research, in which the subsystem of strongly coupled dust particles is used as a model system for the particle-resolved investigations of classical generic phenomena of condensed matter physics.[9,10] These experiments target such fundamental interdisciplinary questions as, for example, electrorheology[11] or turbulence.[12] To be individually resolved, the dust particles have to be sufficiently large. Their size must be in the micrometre range. For such large particles, the gravitational force becomes very important. Although many generic phenomena can be studied in 2D monolayers of dust particles under ground laboratory conditions, the unstressed 3D dust suspensions can only be studied in microgravity. Microgravity experiments are therefore the most ambitious in this field. Under microgravity conditions, the dust particles occupy significant fraction of the plasma volume, and dust–plasma interactions become therefore very important. In spite of the great scientific success of the complex plasma laboratories on the International Space Station (ISS)—PKE-Nefedov,[13] PK-3 Plus[14] and PK-4[15]—the microparticle suspensions observed in these experiments are in a certain parameter range very far from the desired condition of calmness and uniformity.[16–18] Understanding of the fundamentals of dust–plasma interactions is the key to the progress in the quality of the microgravity complex plasma experiments as well as to the correct interpretation of their results.

Our review is dedicated to the physical aspects of dust–plasma interactions. Under the "physical aspects," we understand such phenomena classes, for which the size and chemical composition of dust particles as well as chemical composition of the plasma may be treated as constant in time. This means, we a priori exclude all the effects related to the growth or sputtering of dust in plasmas. Also, we limit ourselves to the consideration of the two discharge types, namely, to the dc discharge and to the capacitively coupled rf (CCRF) discharge. The former is the basis of the present microgravity laboratory PK-4, whereas the latter was extensively used in both microgravity and dust growth research.

We will use the following terminology throughout our review. We will term the plasmas containing dust as "dusty plasmas." This term, in our opinion, appeals to a broader community of plasma physicists[1] compared with the term "complex plasmas." Only in cases, when the dust component of the plasma consists of industrially manufactured particles of regular shape and definite chemical composition, we will term the dust component as "microparticles" and a single particle as a "microparticle." In all other cases, we will apply the terms "dust" or "dust particles" to the dust component and "dust particle" to a single particle, respectively. Established terms like, for example, "dust component," "dust–plasma interactions" or "dust acoustic wave" will be used irrespective of the source and nature of the nano- or micrometre-sized solid particles immersed in plasmas.

The review is organized as follows. In Section 2, we will discuss the elementary processes involving dust particles in plasmas. In Section 3, we will explain the approaches to the numerical simulations of dc and CCRF discharges containing dust. Description of the discharge configurations and diagnostic methods used in the investigations of dust–plasma interactions will constitute the content of Section 4. The phenomena of dust–plasma interactions common for the two discharge types will be reviewed in Section 5. Section 6 will be dedicated to the discharge-type-specific effects of dust–plasma

interactions. Such phenomena as void, heartbeat instability or dust-induced stratification will be considered in it. In Section 7, we present our view on the future directions in the investigations of dust–plasma interactions.

2 | BASIC PROCESSES

Interaction of dust particles with low-temperature plasma is a complex phenomenon that involves several basic physical processes. The most important of them are charging and screening of dust particles as well as momentum and heat exchange between the dust particles and other plasma components. The specific features of these processes depend on the discharge type, operating conditions, and type of dust structure. The important physical factors that influence dust–plasma interactions include plasma collisionality (mainly ion-neutral collisions), anisotropy caused by ion drift flows, and strong coupling between ions and dust particles (nonlinear screening effects).

2.1 | Particle charging

The dust particles in low-temperature plasma usually acquire high negative charges ($\sim 10^3 a_{\mu m}$ elementary charges, where $a_{\mu m}$ is the dust particle radius expressed in μm) due to the collection of ions and electrons. The particles become charged negatively because the mobility of electrons is much higher than that of positive ions. The stationary value of the dust charge can be calculated from the balance equation

$$\sum_{\alpha} J_{\alpha} = 0, \tag{1}$$

with J_α being the currents of different plasma components at the particle surface. Equation (1) is typically used to find the particle surface potential, φ_p. The particle charge, q_p, is then estimated using the simple identity $q_p = 4\pi\varepsilon_0\varphi_p a$, with a being the particle radius. The particle charge depends on the gas type, the ratio of the ion to electron temperatures, T_i/T_e, the ratio of the ion to electron number densities, n_i/n_e, and plasma collisionality.

In collisionless plasmas, the collection of ions and electrons by a single dust particle is well described by the orbital-motion limited (OML) theory.[19] Within this approach, the collection cross-sections for ions and electrons are derived from the analysis of their trajectories in the central field of a charged particle taking into account the conservation of energy and angular momentum. The ion and electron currents are calculated by averaging the collection cross-sections over an appropriate velocity distribution function. Despite known limitations,[20] the OML theory provides a reliable estimate for the particle charge under conditions where the mean free path for ion-neutral collisions, λ_{in}, is much longer than the characteristic screening length (Debye length), λ_D, in plasma.

In weakly collisional plasmas, where $\lambda_{in} \sim \lambda_D$, the ion-neutral collisions affect the ion orbital motion and increase the probability of ion absorption by the dust particle. This increases the ion current to the particle and decreases the absolute value of particle charge. The reduction of particle charge due to ion-neutral collisions has been measured experimentally in dc discharge plasma.[21] Several analytical models were proposed[22–24] to calculate the ion flux in the weakly collisional regime. Self-consistent numerical simulations of dust particle charging in collisional plasma were performed by Zobnin,[25] Lampe,[26] Hutchinson and Patacchini,[27] and Semenov.[28,29] The simulations of Zobnin, Hutchinson, and Patacchini were based on the particle-in-cell approach combined with the Monte-Carlo collisions model, whereas Lampe used a semi-analytical model based on integral expressions for the ion current near the particle. The simulations of Semenov were based on the direct numerical solution of kinetic equations for plasma components using model collision integrals. The comparison between available experimental data, results of simulations, and analytical approximations for the normalized particle potential, $z = e|\varphi_p|/kT_e$, in collisional plasma is shown in Figure 1. It can be seen that the existing analytical models provide sufficiently accurate approximation to the dependence of particle potential on the collisionality parameter λ_D/λ_{in}.

In the highly collisional regime with $\lambda_{in} \ll \lambda_D$, the charging process is well described by the fluid (drift-diffusion) models.[31,32] However, this regime is not relevant for most of the dusty plasma experiments.

2.2 | Screening of dust particles

A charged dust particle immersed in a plasma is screened by ions and electrons. Accurate prediction of the electrostatic potential distribution around dust particles is important for analysing collective effects in dusty plasmas as well

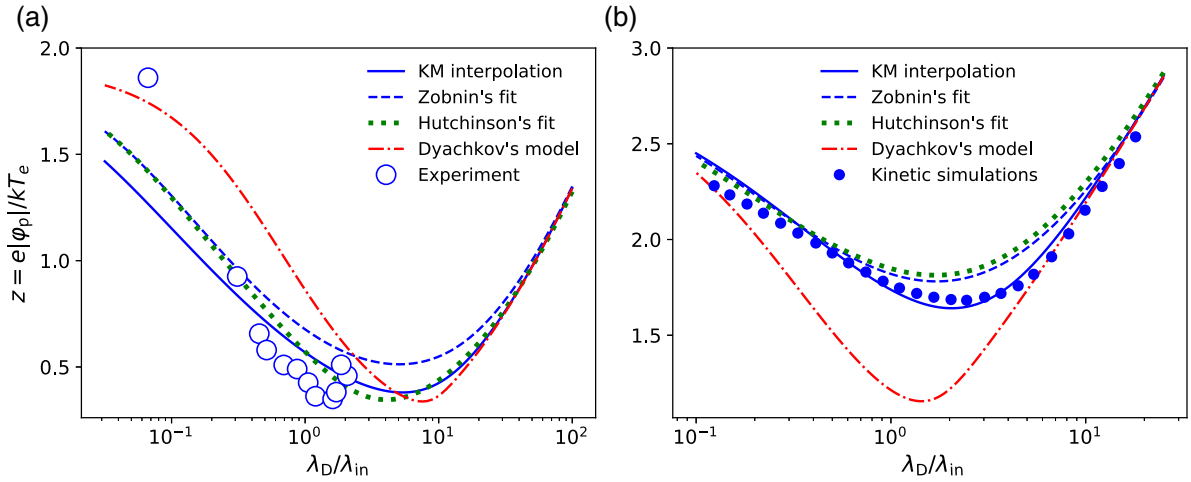

FIGURE 1 Normalized particle potential, $z = e|\varphi_p|/kT_{rme}$, as a function of the collisionality parameter. The results in panel (a) are obtained for the neon plasma, $a = \lambda_D\sqrt{1 + T_e/T_i}/1490$ and $T_e/T_i = 220$. The results in panel (b) are obtained for the argon plasma, $a = 0.1\lambda_D$ and $T_e/T_i = 30$. The presented analytical approximations include the Khrapak–Morfill (KM) interpolation formula,[24] Zobnin's fit,[23] Dyachkov's model,[22] and Hutchinson's fit.[27] Experimental points show the data obtained by Ratynskaia et al.[30] The kinetic simulation results in panel (b) are that obtained by Semenov et al.[29]

as momentum transfer between dust particles and other plasma components. For the case of isotropic collisionless plasma, the exact expression for the charge distribution around an absorbing spherical particle can be derived by solving the Vlasov Equation.[33,34] The electrostatic potential distribution is then obtained by solving the nonlinear Poisson–Vlasov equation. The degree of nonlinearity of the screening process is usually characterized by the parameter $\beta = (a/\lambda_{Di})(e|\varphi_p|/kT_e)(T_e/T_i)$, where λ_{Di} is the ion Debye length. Typically, the following relations hold for the experimental conditions: $\lambda_{Di} \approx \lambda_D$, $T_e \gg T_i$, $e|\varphi_p| \sim kT_e$, and $a \ll \lambda_D$. In most experiments, the nonlinearity parameter $\beta \lesssim 10$; however, it can reach values of the order of 100 for sufficiently large dust particles.[35]

For $\beta \ll 1$, the linearized Poisson equation can be used to describe the screening process. Within the linear model, the potential distribution around the particle is approximated as[36,37]

$$\varphi(r) = \varphi_p \frac{a}{r} \exp\left(-\frac{r-a}{\lambda_D}\right) + \frac{\omega_p}{4}(ak_D)^2 \mathcal{F}(rk_D), \tag{2}$$

where r is the distance to the particle, $k_D = {\lambda_D}^{-1}$, $\omega_p = (kT_i - 2e\varphi_p)/(kT_i + kT_e)$, and $\mathcal{F}(\xi) = [e^{-\xi}\mathrm{Ei}(\xi) - e^{\xi}\mathrm{Ei}(-\xi)]/2\xi$, with $\mathrm{Ei}(\xi)$ being the exponential integral. Note that $\mathcal{F}(\xi) \sim \xi^{-2}$ at $\xi \to \infty$. The first term in (2) is the conventional Debye–Hückel potential and the second term arises due to the absorption of ions and electrons by the particle.

For moderate and high values of β, the linear approximation is not accurate enough. However, in this regime, the Debye–Hückel (Yukawa) potential still yields a reasonable fit to the potential distribution near the particle, provided that the Debye length in (2) is replaced by the effective screening length, λ_s. Several models were proposed to approximate the dependence of λ_s on β.[37–40] According to the recent studies,[37] the effective screening length can be approximated as $\lambda_s = \lambda_D\sqrt{1 + 0.48\sqrt{\beta}}$. For $\beta \sim 1$, this expression can be simplified as $\lambda_s/\lambda_D \approx 1 + 0.24\sqrt{\beta}$. This result is close to that presented in early works.[38,39]

The ion-neutral collisions were shown to affect the far-field behaviour of the potential around an absorbing particle in the isotropic case.[28,29,36] The studies based on a linear kinetic model showed that the asymptotic behaviour of the potential is determined by the Coulomb-like term (i.e., $\varphi \sim r^{-1}$) in the weakly and highly collisional regimes. This result was confirmed by the numerical simulations based on the direct solution of the model kinetic equations.[28,29]

The results obtained for the isotropic case are applicable as long as the ion drift velocity, u_i, is well below the ion thermal velocity, $v_i = \sqrt{kT_i/m_i}$. For example, this condition holds for dust particles in the bulk region of a CCRF discharge. Close to the rf electrodes or in the column of a dc discharge, the ion drift flow is, as a rule, sufficiently strong to cause significant anisotropy of charge distribution around the dust particle. To date, the screening of dust particles in the presence of flowing ions has been predominantly studied using the linear kinetic models[41–43] and particle-in-cell simulations.[42,44] In analogy with the nonlinear effects, the effect of the ion flow can be taken into account by using the effective screening

length for the Debye–Hückel potential.[42,45] For example, the following approximation can be used[45]:

$$\lambda_s = [\lambda_{Di}^{-2}(1+M^2)^{-1} + \lambda_{De}^{-2}]^{-1/2}, \tag{3}$$

where $M = u/v_i$ and λ_{De} is the electron Debye length.

2.3 | Ion drag force and other forces

The scattering of ions by dust particles is known to affect noticeably the dynamics of dust in gas discharges. The drag force exerted on dust particles by drifting ions (ion drag force [IDF]) can be comparable with the electrostatic force caused by the ambipolar electric field in a plasma. For collisionless plasmas, the IDF is typically calculated using the binary-collision formalism.[45–48] Within this approach, the IDF is given by

$$\mathbf{F}_d = m_i \int \mathbf{v} v f_i(\mathbf{v}) \sigma(v) d\mathbf{v}, \tag{4}$$

where σ is the momentum transfer cross-section for ion–dust collisions and f_i is the ion velocity distribution function ($\mathbf{v}$ is the ion velocity and $v = |\mathbf{v}|$). The momentum transfer cross-section for ion scattering on dust particles can be computed numerically assuming that the ion–dust interaction potential is given by the Yukawa potential.[49] In this case, the effective screening length can be used to account for the anisotropy induced by the ion flow and the nonlinear screening effects. Several approximate expressions for the momentum transfer cross-section were proposed by Khrapak et al.[47,48,50] A simple analytical expression for the IDF is available for the case when f_i is given by the shifted Maxwellian distribution.[45] Apart from the elastic scattering process, the collection of ions by dust particles contributes to the momentum transfer cross-section as well. However, this contribution is usually much lower than that associated with the elastic ion–dust collisions.

The effect of ion-neutral collisions on the IDF was studied in detail using the results of particle-in-cell Monte Carlo simulations.[51,52] It was shown that in the weakly collisional regime ($\lambda_{in} \sim \lambda_D$), the IDF slightly increases (by a factor of two) as compared with the collisionless limit. Based on the simulation results, simple correction factors have been introduced to approximate the dependence of the IDF on the collisionality parameter λ_{in}/λ_D. In highly collisional plasmas, the IDF is known to decrease below the collisionless limit.[51–53] According to theoretical models,[54] the IDF can become negative (directed opposite to the ion flow) under some conditions in the highly collisional regime. This effect was confirmed by numerical simulations[51,53] and shown to be caused by the absorption of ions and electrons by the dust particles.

The typical values of the IDF are presented in Figure 2. The estimates are shown for the mobility-limited ion flow under a uniform electric field. The presented results correspond to the conditions of experimental studies performed by Pikalev et al.[55] and Lipaev et al.[16] The IDF is calculated using the same model as that used by Pikalev et al.[55] It is seen that the IDF can be comparable with the electric force acting on the particle for typical experimental conditions.

Apart from the IDF, there are a number of other forces associated with the momentum transfer between the dust particles and plasma components: the electron drag force, the neutral drag force, and the thermophoretic force. The electron drag force was estimated by Khrapak[56] within the binary collision approach. This force can usually be neglected in studying the dust dynamics, except for certain specific conditions in a dc discharge[56] or in case when electron beams of keV energy are introduced into the plasma.[57] The neutral drag force can be estimated using the results from the kinetic theory of gases. Typically, the dust particle size is much smaller than the mean free path for the neutral-neutral collisions in gas. In this case, the neutral drag force can be estimated by the well-known Epstein formula.[58]

The thermophoretic force also plays an important role in the experimental investigations of dusty plasmas. As it is known from hydrodynamics, the thermophoretic force can be estimated using the following expression[59]:

$$\mathbf{F}_{th} = -\frac{4\sqrt{2\pi}}{15}\frac{a^2}{v_n}\kappa_n \nabla T_n, \tag{5}$$

where v_n is the thermal velocity of neutrals, κ_n is the thermal conductivity of the gas, and T_n is the gas temperature.

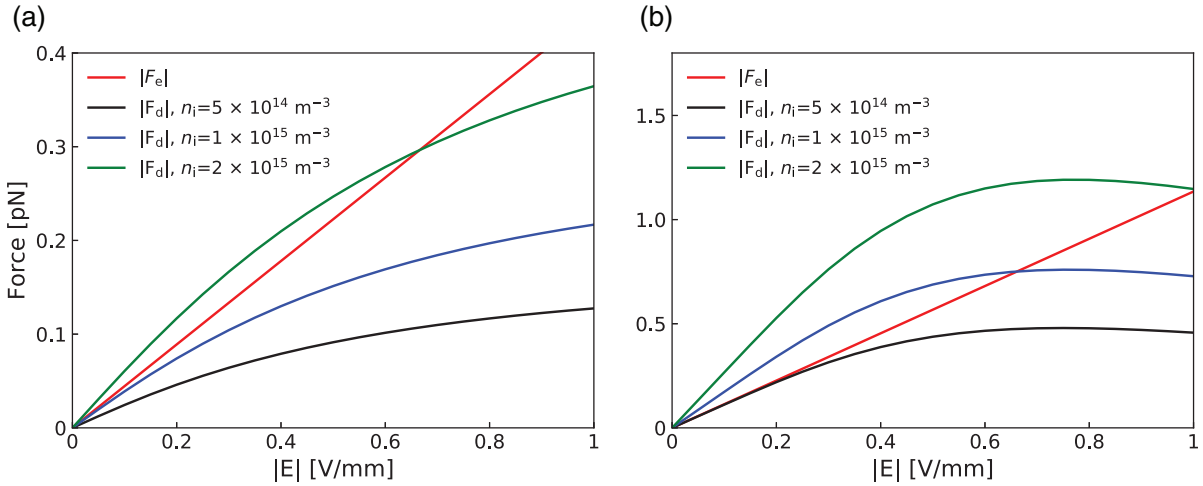

FIGURE 2 The ion drag force, $\mathbf{F}_d$, and the electric force, $\mathbf{F}_e = q_p\mathbf{E}$, for the mobility-limited ion flow. Panels (a) and (b) correspond to the conditions of experimental studies performed by Pikalev et al.[55] and Lipaev et al.,[16] respectively

2.4 | Heating of dust particles in plasma

The temperature of dust particles in plasmas increases due to their interaction with other plasma components. The equilibrium temperature of dust particles can be estimated by considering the balance between the incoming and outgoing energy fluxes. The incoming energy flux includes the kinetic energy contributions of ions and electrons and the energy released due to their recombination at the dust particle surface. Recombination is known to dominate over the kinetic energy contributions.[60] Thus, the incoming energy flux can be estimated as

$$J_{\text{in}} = J_e I_{\text{ion}}, \tag{6}$$

where J_e is the electron flux to the particle ($J_e = J_i$) and I_{ion} is the ionization potential. The outcoming energy flux is mainly determined by the thermal conduction between the gas and the dust particles. According to the results of the kinetic theory, this flux can be estimated as[61]

$$J_{\text{out}} = \pi a^2 \sqrt{\frac{8}{\pi}} \frac{p_g \upsilon_n}{2} \frac{\gamma+1}{\gamma-1} \left(\frac{T_p}{T_n} - 1 \right), \tag{7}$$

where T_p is the dust particle surface temperature, p_g is the gas pressure, and $\gamma = 5/3$. According to the theoretical estimates and experimental measurements,[62] the dust particle temperature can be up to 10–20% higher than the gas temperature for typical experimental conditions.

3 | NUMERICAL MODELS

Processes in low-temperature plasmas can very rarely be adequately described by simple analytical models. Therefore, the physical interpretation of the experiments as well as their design and prediction of the outcome can in most cases be done only on the basis of numerical simulations. The choice of the simulation approach to be used depends on the discharge type and operating conditions. Typically, numerical models of dusty plasma discharges are constructed by extending the existing models of dust-free discharges. The starting point in modelling of CCRF discharges is the use of particle-in-cell simulation technique combined with the Monte-Carlo collision model (PIC-MCC approach) or the use of fluid type models that include transport coefficients obtained from kinetic simulations. The simulations of DC discharges are mostly based on hybrid approaches that combine the kinetic description of electrons, typically based on the non-local Boltzmann equation, and fluid description of ions. The effect of dust particles on the discharge is simulated by using either particle-resolved models or fluid-like description of the dust component.

3.1 | CCRF discharges

The PIC-MCC simulations of CCRF dusty discharges have been presented in a number of works.[63–66] Since the kinetic models are computationally expensive, the existing examples of such simulations are usually limited to the one-dimensional discharge models. In the available simulation codes, the PIC-MCC approach is primarily used to treat the electron component. The ions can be described either by the PIC-MCC approach[64,65] or using fluid models.[66] As it was shown recently,[67] it is possible to construct a fluid-type model that yields sufficiently accurate description of the ion component over a wide range of gas pressures.

The dust subsystem can be described in two different ways. The first approach is based on the description of each single dust particle in the suspension. Such a detailed model is well suited for studying relatively small clusters[64]; however, this approach becomes too computationally expensive for simulating dense large suspensions of dust that are interesting from the point of view of dust–plasma interactions. Therefore, the dust particles are usually described as a continuously distributed component characterized by the local number density.[65,66] Within this approach, the collisions of ions and electrons with dust particles are treated similarly to the electron-neutral and ion-neutral collisions in the Monte-Carlo collision model. The absorption of ions and electrons by the dust particles is implemented using the collection cross-sections taken from the OML theory.[19] The drawback of this approach is that the effect of ion-neutral collisions on the ion flux to the dust particle cannot be taken into account properly, when the ions are described by the kinetic model. In this sense, the fluid description of ions is more preferable. Within the fluid models, the effect of ion-neutral collisions on the absorption of ions inside the dust suspension is easily taken into account using the existing analytical models for the ion flux to the dust particle.[23,24]

The PIC-MCC simulations are useful for analysing the details of electron kinetics in the CCRF dusty discharges. Since the computational cost of these simulations is sufficiently high, the fluid-type models are used to expand the range of problems considered in simulation studies.[63,66,68,69] In particular, fluid models are used to develop the self-consistent description of dust–plasma systems and to extend the available one-dimensional discharge models to two dimension. A typical fluid model represents a closed system of equations for the basic macroscopic parameters of plasma components. The number densities of ions, n_i, and electrons, n_e, are governed by the continuity equations

$$\frac{\partial n_\alpha}{\partial t} + \nabla \mathbf{\Gamma}_\alpha = I_\alpha - G_\alpha, \qquad \alpha = \mathrm{e}, \mathrm{i}, \tag{8}$$

where $\mathbf{\Gamma}_\alpha$ is the particle flux, I_α is the ionization source term, and G_α is the sink term due to absorption of ions and electrons on dust particles. The particle flux is typically defined using the drift-diffusion approximation $\mathbf{\Gamma}_\alpha = n_\alpha \mu_\alpha \mathbf{E} - D_\alpha \nabla n_\alpha$, where $\mathbf{E}$ is the electric field and μ_α and D_α are the mobility and diffusion coefficients, respectively. The electron energy density, $n_\varepsilon = n_\mathrm{e}\varepsilon$, with ε being the mean electron energy, is governed by the energy transport equation

$$\frac{\partial n_\varepsilon}{\partial t} + \nabla \mathbf{\Gamma}_\varepsilon = -e\mathbf{\Gamma}_\mathrm{e}\mathbf{E} + S_\varepsilon, \tag{9}$$

where $\mathbf{\Gamma}_\varepsilon$ is the electron energy flux and S_ε are the energy losses due to elastic and inelastic electron-neutral collisions. The electron energy flux can be approximated as $\Gamma_\varepsilon = \mu_\varepsilon n_\varepsilon \mathbf{E} - D_\varepsilon \nabla n_\varepsilon$, with $\mu_\varepsilon = (5/3)\mu_\mathrm{e}$ and $D_\varepsilon = (5/3)D_\mathrm{e}$. Here, the definition of μ_ε and D_ε is based on the assumption that the electron energy distribution function is Maxwellian. More accurate approximations for μ_ε and D_ε can be obtained from more detailed kinetic analysis.[70]

The transport coefficients for electrons, such as μ_e, D_e, and rate constants for electron-neutral collisions, are usually computed using the local mean energy approximation. Within this approach, the dependence of the transport coefficients on the mean electron energy is predicted by solving the spatially uniform Boltzmann equation. The mobility of ions can be expressed as $\mu_\mathrm{i} = e/m_\mathrm{i}(\nu_\mathrm{in} + \nu_\mathrm{id})$, where ν_in is the ion-neutral collision frequency and ν_id is the effective ion–dust collision frequency. The frequency for ion-neutral collisions is determined using the experimental data or the results of Monte-Carlo simulations.[67,70] The ion–dust collision frequency is closely connected with the IDF acting on the dust particle. From the force balance, one can conclude $\nu_\mathrm{id} = |\mathbf{F}_\mathrm{id}| n_\mathrm{d}/u_\mathrm{i} n_\mathrm{i}$, where n_d is the number density of dust particles, u_i is the ion flow velocity. In many cases, however, the effect of ion–dust collisions on the ion mobility can be neglected. For accurate simulations of the CCRF discharges, the variation of the ion flux within the RF-period has to be taken into account. This is usually done by replacing the actual electric field in the ion continuity equation by the effective electric field.[71] A more consistent approach is based on the solution of the moment fluid equations for ions.[67]

The dust particles can also be described within the drift-diffusion model. In this case, the dust number density is governed by the continuity equation

$$\frac{\partial n_{\mathrm{d}}}{\partial t} + \nabla \mathbf{\Gamma}_{\mathrm{d}} = 0, \tag{10}$$

and the dust particle flux is given by[63,66,68]

$$\mathbf{\Gamma}_{\mathrm{d}} = n_{\mathrm{d}}(m_{\mathrm{d}}\nu_{\mathrm{md}})^{-1}[\mathbf{F}_{\mathrm{id}} + \mathbf{F}_{\mathrm{th}} + q_d\mathbf{E}] - D_{\mathrm{d}}\nabla n_{\mathrm{d}}, \tag{11}$$

where m_{d} is the dust particle mass, q_{d} is the particle charge, ν_{md} is the momentum loss frequency, and D_{d} is the dust diffusion coefficient. The momentum loss frequency is determined by the momentum exchange of dust particles with neutral gas and can be estimated from the Epstein formula.[58] Also, the effective (reduced) values of ν_{md} can be used to speed up the simulations.[66,68] This approach is justified, if only the steady-state configurations of dust structures are of interest. The dust diffusion coefficient, D_{d}, can be estimated using an appropriate thermodynamic model.[63,66,68]

Equations (8)–(10) are combined with the Poisson equation for the self-consistent electric field:

$$\Delta\varphi = -(en_{\mathrm{i}} - en_{\mathrm{e}} + q_{\mathrm{d}}n_{\mathrm{d}})/\varepsilon_0, \tag{12}$$

where φ is the electric potential ($\mathbf{E} = -\nabla\varphi$).

The self-consistent fluid models have been primarily used to study the formation of the central void in the CCRF discharges.[63,68,69] The self-consistent model by Pustylnik et al.[66] is of hybrid type. This model combines the PIC-MCC approach for electrons and fluid description for ions and dust particles. Such hybrid models are useful for studying the effect of dust density distribution on the discharge emission.

3.2 | DC discharges

In case of a dc discharge, the PIC-MCC approach requires large computational resources and its usage is therefore limited. For example, Boef[72] modelled the dc dusty plasma in the approximation of a single cylindrical cell with a given current density and quasi-periodic boundary conditions containing a single dust particle. Only very recently, two-dimensional PIC-MCC simulations were implemented and used for the investigations of a non-stationary and axially non-uniform dc discharge.[73] To reduce the computational effort, hybrid models of dc discharges are typically used. They are based on the solution of the Boltzmann equation for electrons and the drift-diffusion approach for ions. Most of dusty plasma dc discharge simulations are based on hybrid models.

Common approach to the numerical solution of the Boltzmann equation for the electrons in a dc discharge is the so-called two-term approximation,[74,75] which implies weak anisotropy of the electron velocity distribution function (EVDF) in relatively low reduced electric fields. The EVDF is written in the form

$$f(\mathbf{r}, \mathbf{v}, t) = f_0(\mathbf{r}, v, t) + \frac{1}{v}\mathbf{v}\mathbf{f}_1(\mathbf{r}, v, t), \tag{13}$$

where f_0 and $\mathbf{f}_1$ are isotropic and anisotropic components of EVDF, respectively, and $|\mathbf{f}_1| \ll f_0$. The equations for these components
are

$$\frac{\partial f_0}{\partial t} + \frac{v}{3}\nabla_r\mathbf{f}_1 - \frac{1}{v^2}\frac{\partial}{\partial v}\left(\frac{ev^2}{3m}\mathbf{E}\mathbf{f}_1 + \frac{M}{m}v^3\nu f_0\right) + S_{\mathrm{ee}} = -\sum_j\left(\nu_j(v)f_0 - \frac{v'_j}{v}\nu_j(v'_j)f_0\left(\mathbf{r}, v'_j, t\right)\right) + I, \tag{14}$$

$$\frac{\partial \mathbf{f}_1}{\partial t} + v\nabla_{\mathrm{r}}f_0 - \frac{e\mathbf{E}}{m}\frac{\partial f_0}{\partial v} = -\nu\mathbf{f}_1, \tag{15}$$

where ν and ν_j are moment transfer frequency and the frequency of inelastic collisions with an atom in an excited state j (with energy loss of w_j, $v_j' = (v^2 + 2w_j/m)^{1/2}$), respectively, m is the electron mass, e is the elementary charge, $\mathbf{E}$ is the electric field, M is the mass of the molecule, S_{ee} is the electron–electron Coulomb collision operator, and I describes the source and sink of electrons. The electron–electron collisions are usually negligible in the low-current discharge plasma, but can be essential for trapped electrons in the stratified discharge with axial field reversals.[76,77]

In the simulations of dusty dc discharges, the discharge is assumed to be stationary, so the stationary Boltzmann equation is solved. Often, further simplifications are used. EVDF in quasi-uniform electric field can be written as $f_0(\mathbf{r}, v) = n(\mathbf{r}) f_{\text{norm}}(v)$, where $f_{\text{norm}}(v)$ is normalized to the electron density and defined by the Boltzmann equation without spatial derivations.[78–82] An opposite assumption of the large electron energy relaxation length leads to the "global" approach proposed by Tsendin.[83] In this approach, the isotropic EVDF is treated as a function of the total energy of electron ($\varepsilon = w - e\phi(r)$) which is assumed to be constant across the discharge tube radius. Such an approach was used by Sukhinin et al.[84–86] and by Zobnin et al.[87]

Interaction of electrons with dust involves elastic scattering and absorption of the electron by the dust grain surfaces. Emission of electrons from the dust grains is negligible under conditions of the glow discharge plasma.

The drift-diffusion model for ions in dc discharges is essentially the same as that described in Section 3.1. Also, the dust models similar to those described in the previous section can be used.

4 | EXPERIMENTAL TECHNIQUES AND DIAGNOSTICS

4.1 | Discharge configurations

Laboratory complex (dusty) plasmas exist in quite a narrow range of background plasma densities 10^{14}–10^{16} m^{-3}. The lower boundary is determined by the possibility to sustain a discharge with the dust immersed in it. Above the upper boundary of this range, most of the conventional materials of the dust particles do not withstand the heat load from the plasma. Typical electron temperatures are of the orders of a few electron volts. Ionization degree is usually very low ($10^{-5} - 10^{-7}$) and the neutral gas remains cold. Due to ambipolar diffusion, the bulk plasma acquires positive electrostatic potential with respect to the chamber walls and can therefore trap negatively charged dust particles. In the following, we consider technical possibilities of creating such plasmas.

4.1.1 | DC discharge

In the ground-based dusty plasma experiments, the dc glow discharge[88] is usually used in the stratified regime.[89–91] Striations are the ionization instabilities of the positive column of the dc discharge.[92] In the noble gas discharges, striations are usually running with the typical frequencies of tens of kHz. To produce standing striations, which are necessary to trap the dust under the ground laboratory conditions, the discharge channel is locally constricted using a dielectric insert.[89–91] The standing striations then appear on the anode side of this constriction. For ground-based experiments, the glow discharge is usually created in a long, vertically oriented glass tube with two electrodes. Cathode is located at the bottom of the tube and anode—at the top.

Microgravity experiments, in which the interaction between the microparticles and the plasma reveals itself much stronger than in ground-based experiments, were (with the exception for very first attempts[93,94]) conducted in a uniform dc discharge in the PK-4 facility, which is presently operational on board the ISS.[15] Before being launched into space, the scientific performance of PK-4 was tested in nine parabolic flight campaigns.[95–97].

In the PK-4 setup (Figure 3), the dc discharge is produced in a Π-shaped tube with the diameter of 3 cm. The length of the working area is 20 cm. The microparticles can be introduced into the plasma at the edges of the working area from six different dispensers. In PK-4, the discharge with the current up to 3 mA is created between the passive and active electrode located at the edges of the Π-shaped tube. It can operate in dc, as well as in the polarity switching mode. The polarity can be switched with the frequency of hundreds of Hz. Such a frequency is low in a sense that the dc discharge preserves its nature in every half of the period and only changes the direction. On the other hand, this frequency is so high that the microparticles do not react to the oscillations. Using this polarity switching, it is possible to trap the microparticles in the working area of the discharge and to avoid their unipolar drift in the dc electric field.

Both in ground-based and microgravity experiments, the noble gases (mostly neon and argon) are used. Typical pressure is a few tens of Pa.

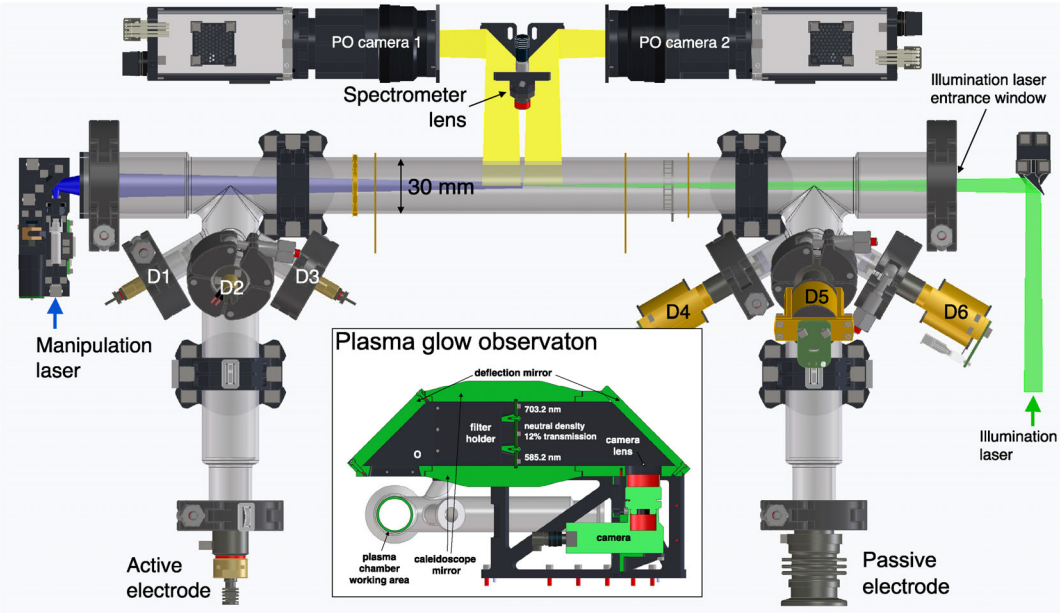

FIGURE 3 Schematic of the PK-4 experiment.[15] The plasma glow observation system is shown in the inset

4.1.2 | CCRF discharge

CCRF discharge[98] was also used both in ground-based and microgravity research. Early experiments used the parallel-plate geometry with one rf electrode and one grounded electrode.[99,100] In more modern experiments, both electrodes are rf-driven[64] in the push-pull mode. Sometimes, rf voltage is applied to a disc-shaped electrode with respect to a grounded cylindrical chamber.[101] Different modifications of a standardized chamber, Gaseous Electronics Conference radio-frequency reference cell,[102] are also widely used in dusty plasma research.

Two generations of microgravity complex plasma facilities on the ISS employed the CCRF discharge: PKE-Nefedov[13] and PK-3 Plus.[14] In both facilities, the discharge was created inside a glass box closed with two parallel metallic flanges, on which the rf electrodes were mounted. The distance between the electrodes was 3 cm. Their diameter was increased from 3 cm in PKE-Nefedov to 6 cm in PK-3 Plus.

The next-generation complex plasma facility COMPACT[103] (formerly, EKoPlasma[104]) is presently under development. It will also be based on the CCRF discharge with more complicated geometry compared with its predecessors. Each of its two parallel-plate electrodes will consist of two concentric, individually powered segments. It will be possible to vary the phase differences between all the four segments as well as to drive the segments in pulsed and continuous modes. Also, the distance between the electrodes will be variable. These improvements will certainly give the experimenter new possibilities in the microgravity conditions (e.g., by extending the accessible range of plasma parameters). However, since the dust–plasma interactions were not yet investigated in this facility, we leave it out of the scope of our review.

CCRF discharges used for the investigations of dust–plasma interactions are usually a single frequency of 13.56 MHz. A RF generator is connected to the electrode via a matching network, which adjusts the impedance of the load to that of the generator.

4.2 | Dust particles

4.2.1 | Sources

In case of CCRF discharge, in many experiments, the dust particles were grown inside the plasma (Figure 4a). For that, the discharge was produced in a reactive gas (e.g., silane[99]) or mixture of gases, such as argon-silane,[107,108] argon-acetylene,[109–114] or argon-methane.[110,111] As long as the size of the grown carbonaceous or silicon-based particles lies in the sub-micron range, the gravitational force is negligible for them and they occupy the entire plasma volume and,

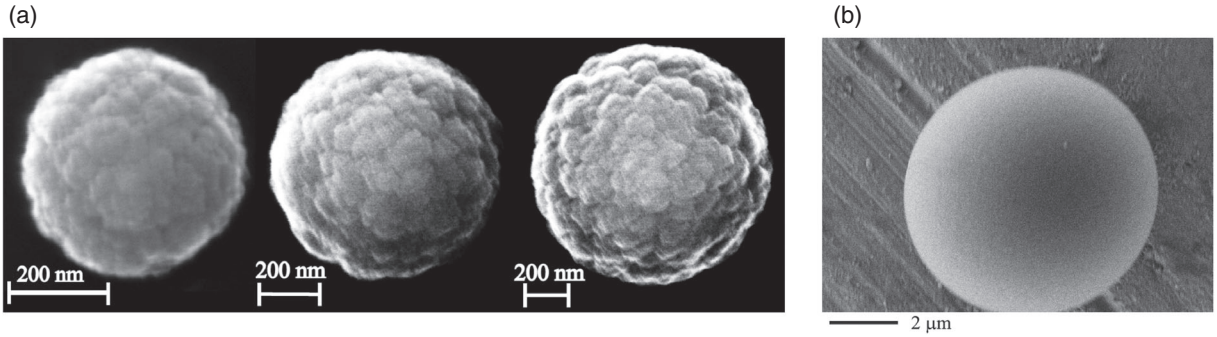

FIGURE 4 (a) Scanning electron microscopy images of dust particles of different sizes synthesized in an argon-acetylene discharge.[105] (b) Scanning electron microscopy image of an industrially manufactured melamineformaldehyde microparticle of 7.3 ± 0.4 μm nominal diameter. Reproduced with permission.[106] Copyright 2016, Pleiades Publishing Ltd.

therefore, dust–plasma interaction effects become prominent. Due to massive contaminations that the reactive plasmas produced in the vacuum chambers, this method of dust generation is usually used under laboratory conditions.

Instead of growing dust in the plasma, it is possible to inject industrially manufactured microparticles (Figure 4b) into it. With the exception for a few works, where the behaviour of nylon microrods in plasmas was studied,[115,116] plastic (melamine-formaldehyde,[15] polystyrene,[105] polymethylmetacrelat[117]) or silica[118,119] microspheres are used as microparticles. These microparticles are kept inside the vacuum volume in special small reservoirs and can be injected into the plasma through the sieve by shaking those reservoirs. Shaking can be performed manually[89–91] (e.g., with the help of a magnet), but under microgravity conditions, the electromagnet shakers are used.[13–15,97]

In some experiments, the dust particles were grown by sputtering the injected microparticles attached to the electrodes.[120,121]

4.2.2 | Thermophoretic levitation of microparticles

Under the ground laboratory conditions, larger (diameter more than 1 μm) dust particles concentrate themselves in the sheath region of the plasma where the dust levitation condition can be satisfied. This makes it impossible to perform laboratory investigations of dust–plasma interactions relevant for the microgravity conditions without implementing a plasma-independent technique. Studying the dust–plasma interactions during the microgravity experiments is usually compromised for the reasons of limited experiment time, dimensions, and/or weight of necessary plasma diagnostics.

A plasma-independent levitation technique was for the first time implemented by Rothermel et al.[122] and used in many other subsequent works on dust–plasma interactions.[55,65,66,123–125] It employs the thermophoretic force (see Section 2.3). To levitate the microparticles thermophoretically, the bottom electrode assembly of the parallel-plate CCRF discharge was heated up by an electrical heater, whereas the top electrode assembly was cooled down with fans (Figure 5). The glass chamber between the electrode assemblies provides the thermal isolation. The heater is controlled to keep a certain temperature difference between the electrode assemblies. Temperature difference of a few tens of Kelvins allowed to levitate micrometre-sized microparticles.

Up to now, the usage of this technique is limited to the CCRF discharge only. However, thermophoresis is not a plasma effect and can in principle be used irrespective of the discharge type.

4.3 | Electrical diagnostics

4.3.1 | External circuit

For any discharge, measurements of the parameters of the external circuit (i.e., discharge voltage, current, and deposited power) are the most basic type of diagnostics and is therefore necessary in any experiment for two reasons. First, the parameters of the external circuit can be controlled by the respective power supplies. Therefore, their precise knowledge allows to reproduce the experimental conditions. Second, parameters of the external circuit are often used as boundary

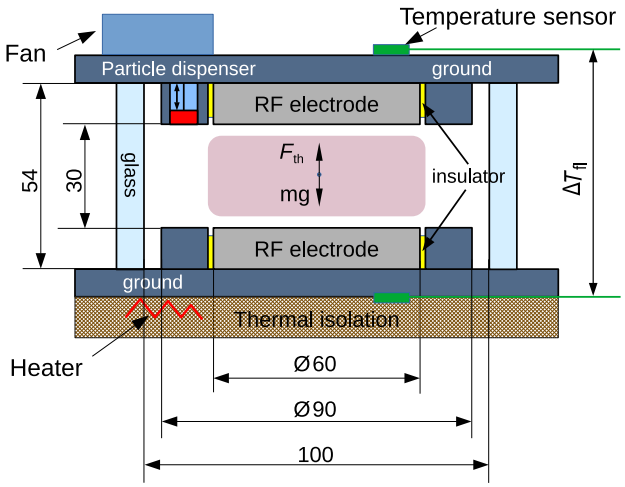

FIGURE 5 Laboratory PK-3 Plus[14] chamber with thermophoretic compensation of gravity. Details of the setup can be found in a paper by Rothermel et al.[122]

conditions in the simulations performed in order to explain (or predict) the outcome of an experiment. External circuit parameters can also be very informative in terms of getting physical insights into the dust–plasma interactions.

In case of a dc discharge, the measurements in the external circuit are straightforward. The current is usually controlled by the power supply and the voltage adjusts itself according to the plasma conditions. The voltage is in most cases determined by the cathode voltage fall and is therefore not affected by the presence of dust. Therefore, sometimes, additional floating electrodes are introduced into the plasma that allow to measure the voltage drop in the vicinity of a microparticle suspension.[126]

For CCRF discharges, diagnostics of the external circuit is a way more complicated task compared with that for the dc discharge. In the electrotechnical sense, plasma is a strongly nonlinear load. Therefore, in an rf circuit, it will generate numerous harmonics. To measure them properly, the measurement probes have to undergo broadband rf compensation and calibration.[102,110,127] Except for the amplitude values of voltage and current, the parameters of interest for the dust–plasma interactions can be the phase angle between voltage and current,[99,108,110] amplitudes of higher harmonics,[128] dc self-bias of an rf electrode,[129] or plasma impedance.[130]

4.3.2 | Langmuir probe

Although the Langmuir probe is potentially one of the best plasma diagnostics in terms of simplicity-to-informativity ratio,[131] its usage in dusty plasmas encounters significant problems. The surface of the probe tip gets contaminated with dust particles. Two strategies were used to mitigate this issue. First was using the fact that the negatively charged dust particles attach to the probe tip when it is positively biased.[132] To minimize the duration of positive bias, the voltage was applied to the probe tip not as a conventional ramp, but using a random sequence. This minimized the duration of positive bias and therefore the attachment of dust to the probe tip. The second strategy was simply to minimize the exposure of the probe tip to the plasma.[133] When not used, the probe tip was covered by a motorized protective cap. In both the cases, the current–voltage characteristics could be obtained and the plasma parameters could be measured. The second strategy even allowed the measurement of the electron energy distribution function.

Nevertheless, the usage of Langmuir probes in dusty plasmas is usually considered as problematic. Contamination of the probe tip is reduced, but cannot be avoided completely[132] requiring periodical ex-situ probe tip cleaning. Also, it was shown that the probe tip significantly perturbs the dust component.[134] In addition, compelling locality of the measurements and constructional difficulties of introducing a Langmuir probe into (usually) small vacuum chambers makes its use for the investigations of dust–plasma interactions unpractical.

In spite of that, the Langmuir probe remains an excellent instrument under dust-free conditions. It can be used for the characterization of dust-free plasmas in support of experiments with dust, as it was done, for example, in the PK-4 project.[15]

4.4 | Microwave diagnostics

Free electrons in low-temperature plasmas are sensitive to electromagnetic waves. This property of plasmas is used in a group of microwave diagnostic techniques, two of which, allowing the measurement of electron density, were used in the investigations of dust–plasma interactions.

4.4.1 | Cavity resonance spectroscopy

A metallic discharge chamber represents (usually a cylindrical) resonator for microwaves.[114,135] For certain frequencies of the microwaves introduced into the chamber (corresponding to transverse electric or magnetic modes), a standing wave will be formed. This diagnostic is usually realized by installing small emitter and receiver antennas inside the chamber. Sometimes,[113] a special cavity with antennas is prepared and placed inside the chamber in the region where it will be exposed to plasma. Emitter is supplied with microwaves whose frequency is scanned in the vicinity of one of the resonances and the amplitude of the receiver signal is monitored. Ignition of the plasma leads to the shift of the resonant frequency which is proportional to the electron density. A combination of microwave cavity resonance spectroscopy (MCRS) with laser photodetachment allows to measure the concentrations of negative ions[113] and, in principle, also charges and densities of the dust particles.

4.4.2 | Interferometry

Another approach in using the microwaves for sensing the free electron density in plasmas is the interferometry.[136,137] Unlike MCRS, it does not require any modification inside the chamber and only requires optical (e.g., through glass window) access to the plasma. Emitter and receiver antennas are placed in front of opposite windows of the chamber. The receiver signal is supplied to the interferometer, where its phase shift with respect to the reference signal is measured. This phase shift will be different in absence and in presence of the plasma inside the chamber. This difference is proportional to the line-of-sight averaged electron density as well as to the length of the path of microwaves in the plasma. The path length can be estimated as the geometrical size of the plasma in the direction of the microwave beam using, for example, optical imaging.

4.5 | Optical diagnostics

4.5.1 | Optical emission spectroscopy

Energetic electrons in plasmas excite gas atoms. Spontaneous decay of the excited states produces radiation which can be spectroscopically analysed. The optical density of dust suspensions is usually not very high, which allows to avoid the multiple scattering problems.[138,139] Intensities of spectral lines, therefore, carry information about the electron energy, electron density, as well as populations of the upper and lower levels of the electronic transitions.[140]

Although the technical realization of the optical emission spectroscopy (OES) is easy and non-invasive, the main difficulty lies usually in the quantification of the results, that is, in obtaining parameters of the emitting medium from the intensities of spectral lines. For $2p \rightarrow 1s$ (in the Paschen notation) transitions of noble gases, which produce the most intensive spectral lines, this results in quite complicated collisional-radiative models.[141–144] However, the importance of qualitative information delivered by the OES should not be underestimated. Spatial profiles of the intensities of the spectral lines[55,99,137,145,146] or change of the ratio of the spectral lines between the dusty and dust-free conditions[147] may contain very important signs for the understanding of the physics of dust–plasma interactions. So-called branching ratio methods[148] can be used to determine the densities of metastable states.[149]

PK-4 contains two spectroscopic tools.[15] First, it includes a fibre spectrometer which allows to perform local measurements in a wide spectral range. The second tool is the three-channel kaleidoscopic plasma glow observation system (see inset to Figure 3). It is designed to observe the entire working area through the narrow-band filters transmitting two different spectral lines of neon. The third channel is equipped with a neutral density filter. All three channels are simultaneously imaged by the same video camera.

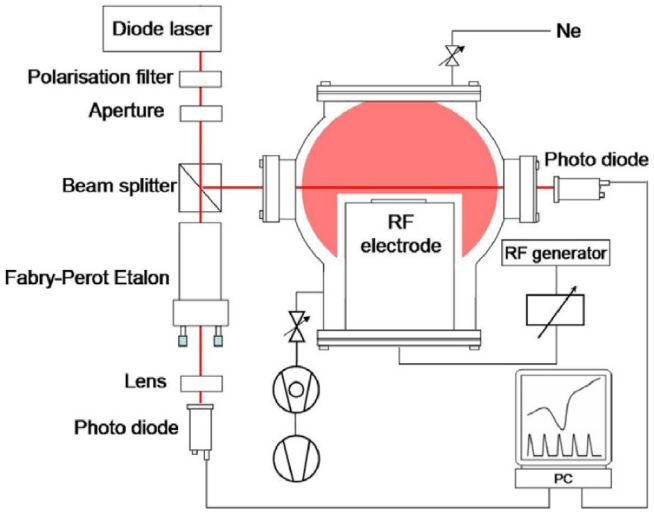

FIGURE 6 Scheme of the laser absorption measurements on $1s_3$ neon metastable atoms in the capacitively coupled rf discharge[155]

CCRF discharge provides the opportunity to look even deeper into the kinetics of excited levels in plasmas, namely, to investigate them with the resolution over the rf period.[150] Using intensified charge-coupled device (ICCD) cameras, it is possible to obtain spatiotemporal profiles of the emission intensities. Since the rf period for the 13.56 MHz signal is about 74 ns, only the spectral lines with the largest Einstein coefficients can be used in this method. In many works on dust–plasma interactions,[55,64–66,151] the so-called rf period-resolved optical emission spectroscopy (PROES) allowed to draw important conclusions.

4.5.2 | Laser spectroscopy

Use of tunable lasers allows to significantly increase the quantitative outcome of optical diagnostics.[152–154] Due to extremely narrow spectrum of the laser radiation (usually in MHz range), the spectral width of most of the Doppler-broadened lines becomes accessible. This opens up the possibilities of measuring the velocity distributions of plasma components as well as precise measurements of their densities.

Laser spectroscopy can be performed either in absorption or in fluorescence configuration. In the absorption configuration (an example of an experimental setup[155] is shown in Figure 6), usually termed as laser absorption spectroscopy (LAS), the spectral dependence of the absorption of the laser beam passing through the plasma is measured. In the fluorescence configuration, usually termed as laser-induced fluorescence (LIF), the spectral dependence of the plasma fluorescence is measured. The advantage of LIF is its imaging ability, although the so-called laser power saturation issues[156,157] and absorption of the laser beam make it much more difficult to obtain reliable quantitative data compared with LAS.

Application of laser spectroscopy to the investigations of dust–plasma interactions does not have a long history. Nevertheless, several works have been performed on $1s_5$ argon metastable atoms[125,149,157–159] and $1s_3$ neon metastable atoms.[155]

One of the unsolved problems that could lead to significant progress in the investigations of the dust–plasma interactions is the measurement of ion velocity distributions. In general, the measurements of ion velocity distributions in low-pressure plasmas are performed using the metastable states of noble gas ions.[160] Therefore, measurements are only possible at low gas pressures (~0.1 Pa)[161,162] and become difficult (because of frequent charge-exchange collisions) in the Pa or tens of Pa range, where the dusty plasma experiments are mostly performed.

It is often believed that laser spectroscopy of plasmas is a non-invasive tool. This is practically true for LAS, where the laser beams are usually attenuated to μW powers to guarantee the linearity of the absorption. However, in the LIF regime, where the transitions must often be saturated by the laser radiation, it is not very difficult to disturb the ionization balance. This is the underlying mechanism of the optogalvanic effect.[163,164] It was noticed that in dusty plasmas, dust

particles may respond to low-frequency optogalvanic perturbations.[123] This property of dusty plasmas may also be used for their diagnostics.

4.6 | Diagnostics of dust

Diagnostics of the dust component of dusty plasmas has the goal to measure several quantities: size and chemical composition,[105,112,165–169] positions and velocities of single microparticles,[170–172] their number density, and charge.[21,173–177] Diagnostics of size and chemical composition makes sense only in case they are not known with sufficient accuracy or significantly change during the experiment, that is, when the dust particles are grown in the plasma or undergo significant sputtering. Since we have left the phenomena associated with chemistry or growth/sputtering of dust particles beyond the scope of our review, we apply the same policy to the respective diagnostic methods and concentrate only on those that are important in terms of measuring the quantities relevant for the physics of dust–plasma interactions.

4.6.1 | Positions, velocities, and number density

To make the dust particles visible during the experiments, they are illuminated by lasers. The laser beam is usually shaped into a thin sheet with the help of cylindrical lenses.[14,15,89] In this way, the suspension of dust particles can be illuminated layer by layer.

If the interparticle distances can be optically resolved, identification of the positions of dust particles seems to be a trivial task. The image should be scanned for the presence of bright spots, and the pixels belonging to each spot should be weighted resulting in a central position corresponding to each bright spot, that is, each dust particle. However, if one intends to acquire best possible accuracy, one has to overcome the so-called "pixel locking" problem,[178,179] that is, the situation when the fractional part of the dust particle position (expressed in pixels of the video image) concentrates around certain values. The reason for that is, for example, that a bright spot does not contain enough pixels, or that many pixels are saturated. Identification of the positions of each dust particle in consecutive video images makes it possible to link those positions into trajectories, which allows measurement of particle velocities. This technique is called particle tracking velocimetry (PTV).[180]

If it is impossible to trace the dust particles from frame to frame to measure their velocities, it is possible to try using particle image velocimetry (PIV),[181] a technique adopted from the fluid mechanics research. The classical realization of this technique requires double-exposure images produced with the help of a pulsed illumination laser, which fires two short pulses within the exposure time of the camera. Velocities are measured based on the auto-correlations detected in the bins of the image. However, velocities can also be calculated using the correlations in consecutive single-exposure images. A velocity vector is then assigned not to a single microparticle, but to a bin. PIV has been successfully used also in dusty plasmas[172,182–184]; however, PTV, if the quality of the images allows to use it, is more informative.[185]

The laser-sheet illumination allows to measure only two components of the dust particle position and velocity. However, for large volumetric suspensions, it is important to measure the dust particle positions and velocities in three dimensions. The easiest way to perform that is the tomographic scanning, during which the illumination laser sheet and the videocamera are synchronously moved orthogonally to the plane of the video image. This is the oldest and most frequently used technique.[13–15,186–188] Its evident disadvantage is the limited temporal resolution. Therefore, other methods allowing to acquire 3D information instantaneously are being investigated. Among them are, for example, usage of the so-called plenoptic cameras,[189] digital in-line holography[190] and stereoscopy.[191,192] Stereoscopic diagnostics is planned to be a part of the future microgravity complex plasma facility on the ISS COMPACT.[103,104]

If the 3D positions of dust particles can be reliably determined, their number density can be calculated in a straightforward way. However, it is often not the case, especially, for grown dust particles of sub-μm size that cannot be individually resolved. The suspension then has an appearance of a more or less uniform "cloud." Under such conditions, determination of local absolute values of the number density of dust particles becomes a difficult task. However, under the assumption of optically thin suspension and identical shape and size of all the dust particles, the intensity of the light they scatter will be proportional to their number density. This allows to determine the relative spatiotemporal variations of the number density of the dust particles directly from the images of the suspensions.[193,194]

4.6.2 | Charge

In the experiments with dusty plasmas, the charge is usually measured by means of dynamical methods. Dynamical methods can be either passive, for example, use the spectrum of spontaneously excited phonons in a 2D monolayer of microparticles,[176] or active, in which a response of the microparticles to an assumingly known disturbance is observed.[21,173–175,177]

Recently, significant theoretical efforts have been undertaken to explore the possibilities of optical detection of the dust charge. The surplus electrons modify the dielectric permittivity of the dust particle material or its surface conductivity and therefore affect such spectral features of scattering as excitonic resonance[195,196] or plasmon resonance.[197,198] Experimental attempts are still very limited: for example, for the 70- to 90-nm size alumina dust particles immersed in a CCRF discharge,[199] the charge-related shift in the infrared absorption spectra could not be observed.

5 | BASIC PHENOMENA

5.1 | Small amount of dust: Interplay of absorption and electron heating

Although, historically, the researchers first encountered very strong and global effects associated with the presence of large amounts of dust particles in plasmas, we start our review of dust–plasma interaction phenomena with those caused by the presence of relatively small amounts of dust. Under these conditions, the dust particles absorb the plasma species and affect the plasma electric field only locally. The resulting effect can be, however, non-local due to the non-locality of electron kinetics in low-pressure discharges.

First direct experimental evidence of plasma absorption by dust particles dates back to 1970,[200] when it was shown that the duration of the plasma afterglow decreases if plasma contains dust. However, measurements in the steady-state discharges appeared only with the development of the entire field of dusty plasmas.

LAS measurements[155] in a neon CCRF discharge containing a thin (several millimetres) layer of dust showed the appearance of a dip in the axial distribution of the number density of $1s_3$ metastable atoms. The width of the dip corresponded to the thickness of the dust layer. At the same time, the radial distribution of the same metastable atoms measured at the height of the dust layer exhibited a decrease in the central area. Absorption of the metastable atoms by dust was the only feasible explanation.

On the other hand, the absorption measurements on the metastable atoms (performed with a single mirror method)[201] revealed the dust-induced increase of the number densities not only inside the microparticle suspension, but also far above it. Further investigations have shown that the dust–plasma interactions are much more complex even in case of small amounts of dust immersed in the plasma.

It was revealed for the first time by PROES measurements in an argon CCRF discharge[151] that even a very thin layer of microparticles levitating in a discharge causes non-local effect on the plasma. The exact pattern of the dust-induced modification of the spatiotemporal emission profile strongly depended on the microparticle size (Figure 7). For smaller microparticles, the emission was increased at the beginning of the sheath expansion, whereas for bigger particles, it was, on the contrary, decreasing at the beginning of the sheath expansion. Experiments with somewhat larger amount of microparticles[64] confirmed the nonlocal character of the dust–plasma interactions. However, the effect shifted towards the increase of the emission above the microparticle layer for all microparticle sizes. The effect was much stronger for larger microparticles. For smaller microparticles also, strong decrease of plasma emission inside the layer of microparticles was observed.

The microwave interferometry measurements[137] performed above the microparticle layer showed the modification of the electron density. Larger microparticles were found to cause its increase, and smaller microparticles—its decrease. Also, in accord with the later PROES measurements,[64] a decrease of the plasma emission inside the microparticle layer was observed for smaller microparticles. For larger microparticles, the plasma emission was increased in the entire discharge volume.

Interplay of local and non-local effects of dust–plasma interactions was nicely demonstrated by measuring the laser absorption simultaneously at two different positions in a CCRF discharge.[125] In this experiment, two laser beams were used. The measurements were performed at different amounts of microparticles. The lower beam always crossed the microparticle suspension, whereas the upper one crossed the microparticle-free area of the discharge when amount of microparticles was small. As long as the amount of microparticles was small, the absorption of the lower beam was

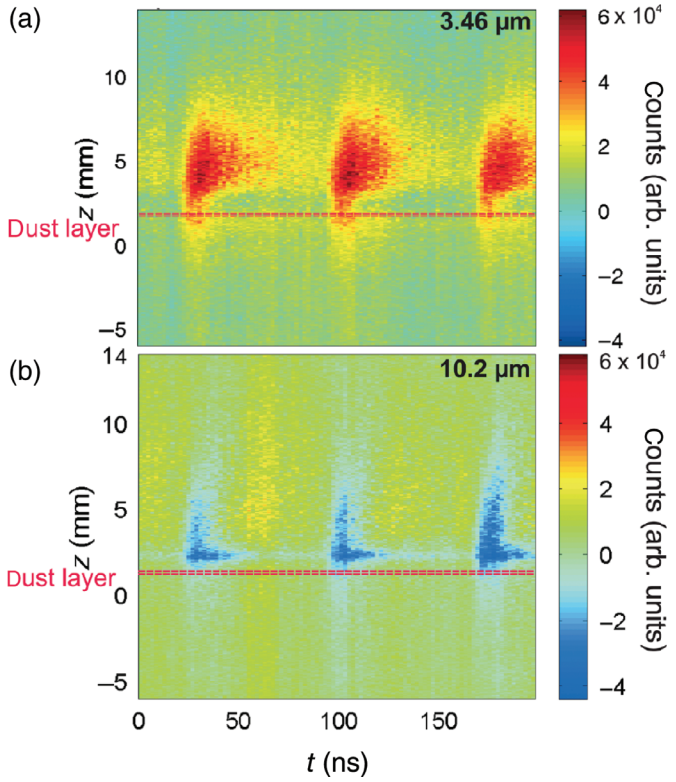

FIGURE 7 Interplay between the plasma absorption on dust and dust-induced non-local electron heating demonstrated using the rf-period-resolved measurements in a capacitively coupled rf discharge. RF discharge power 20 W, argon pressure 40 Pa. The measurement is performed using an ICCD camera through the filter with the central wavelength of 750 nm and spectral width of 10 nm. Microparticles of (a) 3.46 μm and (b) 10.2 μm diameters were used. The spatiotemporal patterns of the difference of intensities between a dusty and dust-free discharges are shown. Reproduced with permission.[151] Copyright 2009, American Physical Society

smaller than in the microparticle-free plasma. However, with the growth of the microparticle amount, the absorption of the lower beam became larger than in the microparticle-free plasma. The non-local effects started, therefore, to prevail over the local absorption. The upper beam, in contrast, always experienced the increased absorption, since the metastable atoms inside it could not be locally absorbed by the microparticles, as their amount was small and the suspension was not reaching the height of the second beam.

The increase of plasma emission and of number densities of metastable atoms above the dust layers levitating in the CCRF discharges suggests that the electrons in that area are excessively heated. The combined three-dimensional particle-in-cell and molecular dynamics model of dust–plasma interactions[64] was able to explain the increase of plasma emission above the dust layer. It was, however, only applied to a single large (10 μm diameter) microparticle in a plasma and, therefore, could not explain the entire variety of the observed phenomena. It can be nevertheless supposed that in all the cases described earlier, the local absorption of plasma species on dust competes with the heating of the electrons by the rf electric field increased due to the immobilization of negative charges inside the dust layer.[65,66] A similar effect is well-known for the electronegative discharges.[202–204]

5.2 | Global influence

5.2.1 | Experimental observations

Already, the earliest experiments in which dust particles were synthesized in the plasma showed the main features of dust–plasma interactions. Bouchoule and Boufendi[145] demonstrated that the growth of dust is accompanied by the reduction of the phase angle between the voltage and current of the CCRF discharge. At the same time, the intensity of

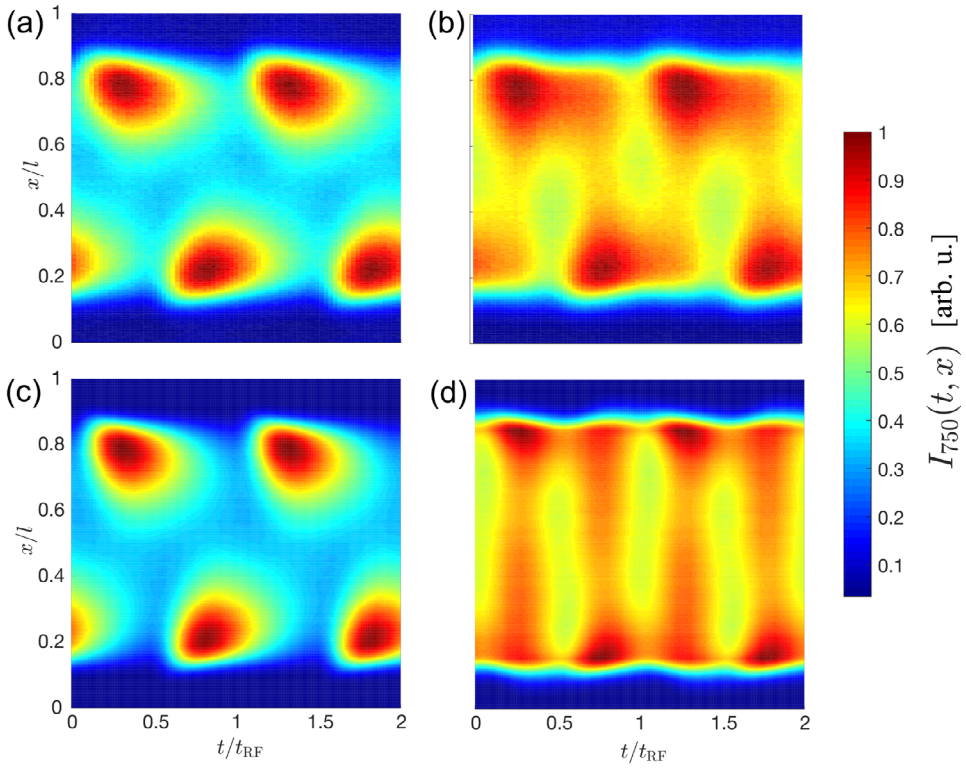

FIGURE 8 Effect of the large amount of dust on the rf-period-resolved emission pattern in a capacitively coupled rf discharge. Measured emission patterns (a) without and (b) with dust as well as simulated emission patterns (c) without and (d) with dust are shown. Experimental results qualitatively agree with the results of the simulations. Discharge in argon at 27 Pa pressure is considered. Amplitude of the rf voltage is 54 V. Further details of experiments and simulations can be found in the paper by Pustylnik et al.[66]

the plasma emission increased,[100,145] and even flattening (of usually two-humped) axial emission profile of a CCRF discharge was observed.[100] Spectroscopic[145] and Langmuir probe[100] measurements revealed the dust-induced increase of electron temperature. The electron and ion densities decreased, whereas the number density of $1s_5$ metastable atoms increased.[145] The observed transition was, in its appearance, very similar to the $\alpha - \gamma$ transition in CCRF discharges[98] and was therefore termed $\alpha - \gamma'$ transition.[205] These findings were confirmed in later works.[109,135,206,207] The investigations of the effect of growing dust on the electrical parameters of the CCRF discharge gave rise to the dust detection techniques and even dust metrology methods which rely on the electrical measurements only and do not require any optics.[128,129]

Further progress in the experiments on CCRF discharges was achieved on the suspensions of industrially manufactured microparticles injected into the plasma. Spatiotemporal patterns of the plasma emission obtained using rf PROES[65] showed that the emission spots associated with the rf sheath expansion, which in the microparticle-free discharge concentrate in the vicinity of electrodes, penetrated much deeper into the plasma and were even able to reach the opposite sheath in the case of a dusty discharge. In a later work[66] which confirmed the result of Killer et al.[65] (see Figure 8), it was shown how this spatiotemporal pattern evolves with the increase of the amount of microparticles in the plasma. PROES observations were therefore in accord with earlier electrical and time-averaged spectroscopic measurements and confirmed the heating of electrons in dusty discharges as compared with dust-free discharges.

Early emission spectroscopy measurements[145] as well as later LAS measurements[208] demonstrated that the presence of dust in CCRF plasmas affects not only the electrons, but also the neutral component. The number density of metastable states increases. Very recent precise LAS measurements[125] revealed another much more important effect of dust–plasma interactions involving the neutral component of a CCRF plasma. It turned out that not only the number densities, but also the temperatures of the metastable atoms are increased in presence of dust. Metastable atoms are in thermal equilibrium with those in ground state and therefore the increase of their temperature indicated the increase of the temperature of the entire neutral component. The increase is relatively small, of the order of several Kelvins, which is negligible for their dynamics. It may, however, play an important role for dust as long as it is subject to thermophoresis.

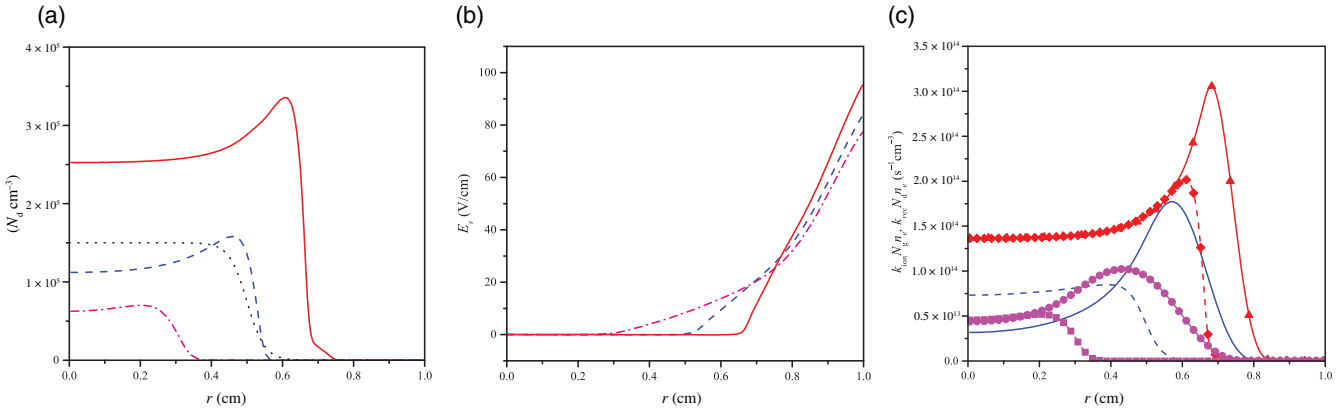

FIGURE 9 Localization of the ionization balance inside a dust suspension immersed in a plasma demonstrated using the hybrid model of the radial confinement of a dust suspension in a dc discharge. Radial distributions of the following quantities are shown: (a) number density of dust, (b) radial electric field, and (c) rates of electron impact ionization and recombination of electrons and ions on the dust particles. Distributions shown with red and purple curves and symbols are self-consistently calculated and correspond to the respective different amounts of dust immersed in the discharge. Blue curves in plates (a) and (b) also correspond to the self-consistent calculations. The dotted line in plate (a) represents a fixed dust configuration, for which the ionization and recombination rates are given with blue lines in plate (c). The following parameters were used in the simulation: argon pressure 1 Torr, discharge current 1 mA, dust particle radius 1 μm, and discharge tube radius 1 cm. Reproduced with permission.[211] Copyright 2013 American Physical Society

Gradients of the order of 1 K/cm may exert significant forces on the microparticles.[15] Therefore, dust-induced modification in the field of the neutral gas temperature should be taken into account in the models describing dusty discharges along with the dust-induced modifications of the parameters of the charged component.

Experimental investigations of the dust–plasma interactions in dc discharges do not have that long history as those in CCRF discharges and were started only in connection with the development of PK-4 microgravity laboratory.[15] Nevertheless, some important findings were also done here. For example, it was shown in a ground-based experiment that the average axial electric field in a striation containing a dust suspension increases up to 25% compared with that in a dust-free striation.[126] In this measurement, the striation is formed between two ring electrodes at a distance of 5 cm from each other (see Section 4.3.1).

Investigations under microgravity conditions revealed several specific phenomena related to dust–plasma interactions[87,186] in the dc discharge which will be discussed in Section 6.1. Here, we would only mention that the spectroscopic investigation of the plasma emission[209] using the plasma glow observation system indicated the increase of the electron temperature in the dusty dc discharge in an analogy to CCRF discharges.

5.2.2 | Physical interpretation

Dust-free low-temperature low-pressure plasmas are usually characterized by the non-local ionization balance. The electron–ion pairs are produced in the bulk by electron impact ionization, whereas the recombination occurs on the walls of the plasma reactor or on the electrodes.[88,210] This leads to the formation of the ambipolar electric field that adjusts the fluxes of electrons and ions in such a way that the quasineutrality can be supported at every point of the plasma.

In presence of dust in the plasma, the ionization balance inside the dust suspension can localize. This was for the first time clearly shown by Sukhinin et al.,[211] who investigated the radial distributions of plasma parameters in a dc discharge. They combined the hybrid model of the dc discharge based on the two-term approximation for the EVDF and drift-diffusion equation for ions[84] with the simple model of dust–plasma interactions. The fluxes of electrons and ions onto the surface of dust particles were calculated using the OML theory.[19] Radial distribution of dust was also calculated using the drift-diffusion approximation taking into account the macroscopic electrostatic force as well as the Yukawa interaction between neighbouring dust particles. It turned out that dust self-consistently arranges in such a way that the radial ambipolar electric field is zero (Figure 9), which is the manifestation of the locality of the ionization balance. This result was confirmed also for the case when IDF was taken into account.[212]

On the other hand, when considering the same problem of the radial stability of the dust suspensions in a dc discharge at considerably larger currents compared with previous works,[211,212] Fedoseev et al.[213] encountered strong (of the order of several V/cm) electric fields inside the suspensions. In this case, the mechanical balance was realized by the detailed balance between the electrostatic force and IDF at non-zero electric field.

Generalizing the results of the simulations by Sukhinin et al.[211,212] and Fedoseev et al.,[213] we can formulate two principles of the self-organization of the microparticle suspensions immersed in low-temperature plasmas in presence of only two dominating forces—electrostatic force and IDF: (a) the ambipolar electric field inside the suspension vanishes. This leads to the trivial force balance for the dust particles and localization of the ionization balance. (b) The ambipolar electric inside the suspension does not vanish. Detailed local balance of electrostatic forces and IDF has to be satisfied for the dust particles. Ionization balance is non-local (as in a dust-free discharge). The parameter that defines the principle is the ionization rate in the plasma (determined by current for the dc discharge). At low ionization rates, the ion fluxes in the plasma are insufficient to compensate the electrostatic force by the IDF, and the suspension self-organizes according to the first principle. Increase of the ionization rate makes the second self-organization principle possible. In Section 6.2.1, we will show how these two principles help to understand the two regimes of void in a CCRF plasma.[55]

In Section 5.1, we have already shown that the presence of even small amount of dust causes non-local excessive heating of plasma electrons. It is therefore not surprising that the same happens when dust occupies significant fraction of the plasma volume. However, the exact physical mechanisms that lead to this heating are different for dc and CCRF discharges.

For dc discharges, this effect was for the first time numerically demonstrated in the previously mentioned simulations by Boeuf.[72] It was shown that the increase of the dust particle size at constant dust density leads to the increase of the electron temperature and, consequently, of the ionization rate. Similar results were obtained for micrometre-sized dust particles by Sukhinin and Fedoseev[86] using their hybrid model,[84] Polyakov et al.[80] using the drift-diffusion model of the discharge, and by Usachev et al.[186] using the modified Shottki theory[88] of the positive column of the dc discharge with local ionization balance inside the dust suspension. These results explain the spectroscopically observed increase of the electron temperature[209] as well as the increase of glow intensity observed in the PK-4 experiment.[87]

The physical mechanism of the excessive electron heating in the dusty dc discharge is connected with the necessity to keep the discharge current constant.[72] The plasma losses on the surfaces of the dust particles effectively result in the increase of the plasma resistance. In order to support the same current as in dust-free plasma, the discharge voltage and consequently the axial electric field in the discharge are increased. This is in accord with the experimentally observed increase of the axial electric field after the injection of dust into a dc discharge striation.[126]

In the CCRF discharge, the other mechanism of excessive electron heating is at work. In a dust-free CCRF discharge, the plasma electrons are heated mainly by the sheath electric field.[98] At the same time, the electrons effectively screen this electric field due to their high mobility. Therefore, ionization and glow are concentrated in the narrow layers close to the sheaths. However, in a dusty CCRF discharge, the free electron density considerably decreases. Their negative charge gets immobilized on the surfaces of dust particles. This allows the sheath electric field to penetrate much deeper into the bulk plasma.

Although the spatiotemporal redistribution of the ionization rate in a dusty CCRF discharge was obtained in PIC simulations long ago,[107] the above-mentioned mechanism was revealed considerably later by Killer et al.[65] In the simulations performed in that work, the static homogeneous distribution of dust in the argon plasma was implemented. A more advanced model that allowed self-consistent fluid treatment of dust component[66] confirmed the above-mentioned mechanism. Spatiotemporal profiles of the plasma emission measured using PROES[65,66] were in agreement with the respective spatiotemporal profiles obtained in the simulations.

Dust-induced spatiotemporal redistribution of the electric field unavoidably leads to the redistribution of the heat sources in the discharge. In this sense, the dust-related non-local temperature increase observed in CCRF[125] is not surprising. Not only electron, but also the neutral gas temperature field in the discharge is modified as a result of dust–plasma interactions. Nevertheless, this issue is very rarely accounted for in the literature and is, therefore, quite poorly studied. On the other hand, we have already pointed out the potential importance of this issue in Section 5.2.1. Based on this, we discuss the state-of-the-art understanding of dust-induced changes of the neutral gas temperature below. There are two dust-related effects that affect the neutral gas temperature: (a) redistribution of the heat source associated with the elastic electron-neutral and ion-neutral collisions (existing also in the dust-free plasma) and (b) heat exchange between the dust particle surface and neutral gas (see Section 2.4 and references therein).

Perrin et al.[214] were the first to discuss the self-consistent neutral gas temperature in a dusty discharge. According to their calculations, appearance of dust in a plasma leads to a significant (~10 K) increase of the temperature difference

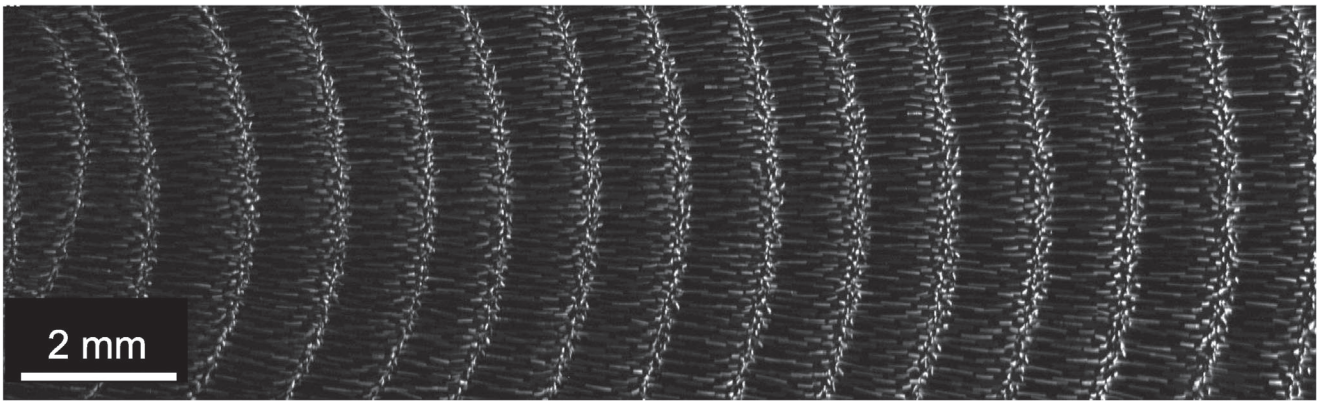

FIGURE 10 Dust acoustic wave instability observed in the PK-4 experiment under microgravity conditions[194]: discharge current 1 mA, neon pressure 38 Pa, and microparticles of 3.34 μm diameter

between the central area of the plasma and the walls of the reactor. Their conclusion was: "for isolated particles of $r_p = 50$ and 500 nm in a pristine Ar discharge, ion drag is the dominant force pushing particles from the plasma centreline to the sheath edges, but in a dusty discharge of $r_p = 50$ nm, plasma-induced thermophoresis dominates the ion drag and electrostatic forces due to the vanishing DC ambipolar electric field in the plasma bulk."

According to the simulations by Akdim and Goedheer,[215,216] the influence of the plasma-produced temperature gradients on the dynamics of micrometre-sized dust is in general negligible. In spite of this conclusion, the models in the subsequent papers of that research group[63,217–219] always contained the heat balance for the neutral gas as well as the thermophoretic force.

In contrast to that, a very simple drift-diffusion discharge model by Vasilyak et al.[79] (similarly to Perrin et al.[214]) exhibited rather a strong dust effect on the neutral gas temperature field.[220] The radial neutral gas temperature distribution in a dc discharge was considered in this work. The dust configuration was considered static. The cylindrically shaped dust suspension occupied half of the diameter of the discharge tube. The model exhibited a 2 K jump in the axial value of the neutral gas temperature when changing from $n_d = 0$ to $n_d = 10^{11}$ m^{-3}.

We can therefore state that the issue of dust-induced changes in the neutral gas temperature fields is at the moment rather controversial. It requires much more experimental as well as computational attention for the final conclusion of its importance for the self-consistent dynamics of dust in plasmas.

5.3 | Dust acoustic wave instability

Up to now, we considered the phenomena of dust–plasma interaction that do not affect the dynamics of dust. However, it was demonstrated long ago[221] that dust immersed in a gas discharge plasma does not necessarily remain in the thermal equilibrium with neutral gas. Moreover, in dusty plasma, there exist several instabilities that induce different types of regular dust motion,[17,18,120,147,222–235] some of which will be considered in this review.

Dust acoustic wave (DAW) [236] instability is definitely the most common type of instability occurring in laboratory dusty plasmas. Low-frequency oscillations of the plasma emission and dust-scattered light intensities were for the first time observed by Chu et al.[237] in a dust-growing silane-argon-oxygen CCRF discharge and were immediately interpreted as DAW.[238] Very soon after that, the first images of DAW were obtained in the experiments in a Q-machine.[239] The instability reveals itself as a compressional wave pattern propagating in many cases along the local electric field. DAW instability is really a ubiquitous phenomenon occurring in practically all types of discharges—dc,[240,241] inductively coupled rf,[193,242] and CCRF[243]—under laboratory[244] and microgravity[194,245] conditions, with injected microparticles[246] and grown dust.[247]

In spite of the broad abundance of situations supporting the DAW instability, we will not go deep into its theory and refer the interested reader to the papers published within the recent 30 years.[193,243,248–256] We will instead concentrate here on the most important issues in understanding the physics of the DAW instability.

In 1990, Rao, Shukla, and Yu showed that dusty plasmas can support acoustic wave mode in a similar manner as normal electron–ion plasmas support ion acoustic waves.[257] For collisionless, isotropic dusty plasmas, in the acoustic limit, the phase velocity of the waves tends to the value:

$$C_{\mathrm{da}} = \omega_{\mathrm{pd}} \lambda_{\mathrm{D_i}} = \sqrt{\frac{Z_{\mathrm{d}}^2 k_{\mathrm{B}} T_{\mathrm{i}}}{m_{\mathrm{d}}} \frac{n_{\mathrm{d}}}{n_{\mathrm{i}}}}. \tag{16}$$

Presence of m_{d} in the denominator suggests that these velocities are very low. Indeed, for the real experimental conditions C_{da} acquires the value of several cm/s. It was supposed that DAW may propagate in natural dusty plasmas (e.g., in the Saturn rings or in terrestrial noctilucent clouds), which possess the above-mentioned properties of isotropy and absence of collisions.

On the contrary, in the dusty plasma experiments, it is very difficult to satisfy those two conditions. Electric fields, relatively high neutral gas pressures, and large dust charges do not allow to consider the plasma isotropic and its dust component collisionless. In a real experiment, the Rao–Shukla–Yu mode would be very quickly damped by the neutral drag force. Only the presence of DAW instability makes the propagation of a compressional wave mode possible in the laboratory dusty plasmas.

The DAW instability is the ion streaming instability that occurs when the ion flow is driven through dusty plasmas. For the instability to occur, the drift velocity of the ions u_{i} must be greater than the velocity of the wave mode they are supposed to support. In case of DAW this condition may be understood as $u_{\mathrm{i}} \gtrsim C_{\mathrm{da}}$. However, in a real experimental situation for the instability to occur, its increment has to exceed the Epstein damping rate. Therefore, in the laboratory gas discharge plasmas, DAW are excited at much larger ion drift velocities.

The critical electric field, required for the onset of the DAW instability, can be expressed as follows[251]:

$$E_{\mathrm{cr}} \approx \frac{k_{\mathrm{B}} T_{\mathrm{i}}}{e \lambda_{\mathrm{D_i}}} \left[\left(\frac{\omega_{\mathrm{pd}}}{\nu_{\mathrm{md}}} \right)^2 + \left(\frac{\omega_{\mathrm{pi}}}{\nu_{\mathrm{in}}} \right)^2 \right]^{-1/2}, \tag{17}$$

where ω_{pi} and ω_{pd} are the ion and dust plasma frequencies, respectively, and ν_{in} is the frequency of ion-neutral collisions. Fink et al.[258] have reduced this equation to $E_{\mathrm{cr}} \sim k_{\mathrm{B}} T_{\mathrm{i}} \nu_{\mathrm{md}} / e C_{\mathrm{da}}$ implying that $\omega_{\mathrm{pd}}/\nu_{\mathrm{md}} \gg \omega_{\mathrm{pi}}/\nu_{\mathrm{in}}$; however, in reality, these two values may be of the same order. Typical values of E_{cr} lie in the V/cm range.

Piel et al. showed both experimentally and theoretically that the self-excited DAWs can propagate also obliquely with respect to the driving electric field.[252,253] It also turned out that the observed phase velocity is somewhat larger than that predicted by Equation (16).[259] That is attributed to the fact that the ion flow velocity required to excite the instability is larger than the thermal velocity of ions. Therefore, the shielding length will be larger than the ion Debye length λ_{Di} (see Equation 3). For this reason, Piel suggests[259] to term the self-excited compressional waves in dusty plasmas as "dust density waves" instead of "dust acoustic waves." However, in this review, we keep the latter term.

Indeed, the phase velocity of self-excited waves depends on the driving electric field. This was explicitly shown in a microgravity experiment in the PK-4 facility, in which the DAW instability was excited in a microparticle suspension drifting in the dc discharge.[194] The waves in the "head" of the suspension moved faster compared with those in the "tail," reflecting the spatial profile of the electric field predicted by the simulations.[87] Investigations using the PK-4 apparatus also revealed that phase velocity of the self-excited DAW strongly depends on the interparticle interaction potential.[260] In isotropic dusty plasmas, the interaction between the particles is Yukawa-like (see Equation 2). However, in presence of an attractive quadruple term associated with the deformation of the shielding ion cloud by the ion drift,[41] the phase velocity of the DAW decreases.

The importance of the DAW instability for laboratory and microgravity dusty plasma research can be summarized as follows. First, the DAW instability limits the discharge parameter range where calm microparticle suspensions can be investigated. It sets in easier at low neutral gas pressures,[237,240,251] whereas reaching low gas pressures is important to reach the regime of undamped dynamics of microparticles.

Second, as it was shown by Du et al.,[261] DAW instability may lead to agglomeration of dust particles. They have directly measured the velocity distribution of microparticles using the PTV. The calculated collision rate was in accord with the observed time of the appearance of agglomerates in the suspension. The agglomeration collisions during the DAW instability were observed later by Dap et al.[262]

In addition to the two above-mentioned issues, DAW instability can be used for the diagnostics of dusty plasmas.[263,264] To demonstrate this, Tadsen et al.[263] synthesized the dust particles in an argon-acetylene CCRF parallel-plate discharge. Once the particles reached the size of about 0.4 μm, the acetylene supply was stopped and further experiment was conducted in pure argon. The authors have processed a horizontally propagating spatiotemporal wave pattern using the Hilbert transform and obtained the local values of frequencies and wave numbers. Assuming that these values correspond to the most unstable wave mode, that is, to the maximal growth rate, Tadsen et al. were able to derive the local values of ion drift velocities and ion densities. Similar analysis was then later applied to the magnetized dusty plasmas.[264]

6 | SPECIFIC PHENOMENA

6.1 | DC discharge

As already mentioned (Section 5.2.1), the investigations of the dust–plasma interactions in the dc discharge started with the development of the PK-4 facility, in which the dc discharge is essentially used in two modes[15]: (a) steady-state (or unipolar) dc discharge, in which the absolute value and the sign of the current remain constant in time and (b) polarity-switched discharge, in which the polarity of the discharge is changed with the frequency of several hundreds of Hz. Since the frequency of polarity switching is between the typical dust and plasma frequencies, the dust–plasma interactions manifest themselves differently in those two situations. We, therefore, treat these two discharge modes separately.

6.1.1 | Unipolar mode

A dust suspension in the unipolar discharge is subject to rather a fast (cm/s) drift. Therefore, in PK-4, this regime is in most cases used not for the actual experiment, but for the preparatory procedure in which the microparticle suspension is transported from the injection point to the working area. Nevertheless, measurements performed with the glow observation system under microgravity conditions during this transport delivered important information on the dust–plasma interactions.[87]

First of all, the drift of the microparticles was accompanied by the drift of the area of increased plasma emission. Interestingly, plasma emission inside the suspension was maximal in its "head" and was slowly decreasing towards the "tail." In addition to that, the standing striations appeared ahead of the drifting microparticles. Appearance of standing striations in a dc discharge is usually associated with the perturbations in the positive column caused by, for example, a Langmuir probe[265] or sharp change of the tube radius.[266] The discharge on the anode side of the disturbance becomes stratified. We remind that this property is used in the dusty plasma experiments to trap the dust under ground laboratory conditions (Section 4.1.1).

The simulations qualitatively reproduced all the features observed in the experiment.[87] It turned out that the longitudinal electric field inside the drifting suspension increases about a factor of four with respect to the dust-free discharge value in the head of the drifting cloud. In accord with this, the microparticles in the head of the suspension drifted faster compared with those in the tail. Also, the spatiotemporal pattern of the DAW self-excited in a drifting suspension[194] exhibited larger phase velocity in its head compared with that in its tail.

6.1.2 | Polarity-switching mode

Before the start of the actual experiment in the PK-4 facility, the drift of the suspension is stopped by changing the discharge mode from unipolar to polarity-switching. Here, we consider two phenomena of dust–plasma interactions that are specific for the latter regime.

The first one reported by Usachev et al.[186] reveals itself as *partitioning* of the dust suspension. It occurs in the broad range of experimental parameters (especially in neon gas) on the subsecond timescales after changing of the discharge mode to polarity switching (see Figure 11). The uniform suspension drifting in a unipolar discharge is then split into several partitions. The areas of increased plasma emission coincide with the cloud partitions. On the other hand, in case

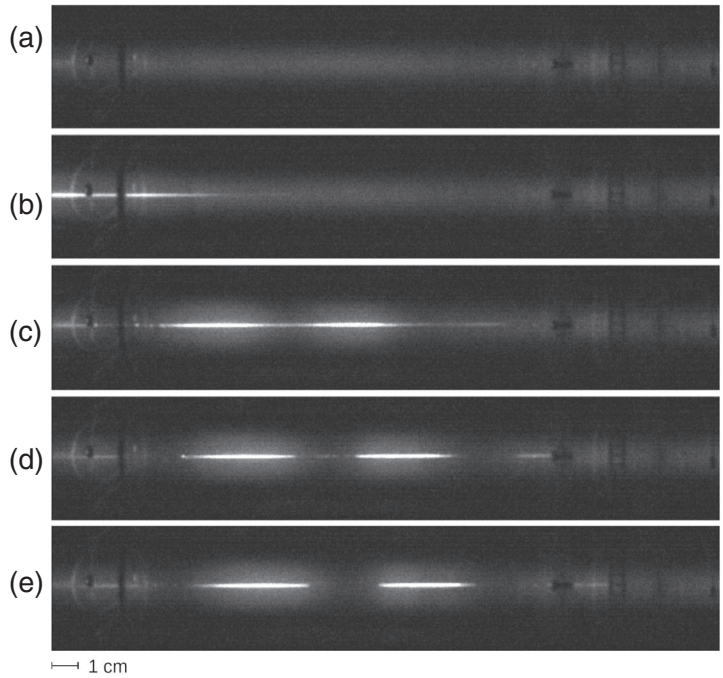

FIGURE 11 Partitioning of the dust suspension in the polarity-switched discharge (1 mA, 40 Pa of neon). The time interval between the images is 2 s. The image is obtained with the plasma glow observation system of PK-4 whose line of sight is almost parallel to the plane of the illumination laser sheet. Thin bright stripe in each image corresponds to the microparticle suspension. (a) Microparticles (3.4 μm diameter) enter the working area on the left; (b, c) the suspension drifts in the dc discharge; (d, e) the suspension gets partitioned in the polarity-switched discharge

of an argon discharge, there exists quite a broad parameter range, in which the microparticle suspensions retain their uniformity even after trapping in a polarity-switched discharge.[187,188]

The mechanism of partitioning remains unclear. Existing models are not able to self-consistently simulate the behaviour of dust in a polarity-switched discharge. The axial confinement of dust in partitions, obviously, cannot be explained in terms of classical concept of ambipolar electric field.

With increase of the amount of microparticles injected into the dc discharge, another phenomenon, which was termed "transverse instability," sets in.[18] It appears as synchronous oscillations of microparticles in the direction orthogonal to the discharge axis. During this instability, the radial profile of the plasma emission looses its symmetry and also starts to oscillate. Both microparticles and the emission oscillate with the same frequency which lies in the range between 10 and 30 Hz.

Theoretical model of this instability was developed by Zobnin et al.[18] The mechanism suggested in that work can be explained as follows. In the area occupied by dust, the electron density is much smaller than in the dust-free area. This creates an ambipolar electric field which pushes the dust into the area of maximal electron density. Due to absorption of plasma on the dust particles, the plasma is "pushed out" of the dusty area. This leads to synchronous oscillations of dust and plasma. It was shown that the development of such oscillations requires the nonlinear dependence of the ionization rate on the electron density. A realistic mechanism providing this non-linearity is the dependence of the electron energy distribution on the local value of the radial ambipolar electrostatic potential.

6.2 | CCRF discharge

6.2.1 | Void

The void is a dust-free area inside a dust suspension immersed in a plasma. It is one of most common disturbances of the homogeneity of CCRF dusty plasmas under microgravity conditions. Void formation and growth also determine the dust particle generation cycle in plasma reactors. It was observed already in early works related to dust growth in reactive[267] or

sputtering[222] plasmas as well as in microgravity experiments.[268] In ground experiments, the void can be obtained using the thermophoretic gravity compensation (Section 4.2.2). It is therefore one of the most extensively investigated physical phenomena of dust–plasma interactions. In spite of significant effort, the mechanisms that control the void formation and provide its stability are still not finally clear.

We will discuss the voids in CCRF dusty plasmas only. We should nevertheless note that the radial void may exist also in the dc discharge. However, as we showed in Section 6.1, the dc discharge dusty plasma rather suffers from other disturbances of non-uniformity. Due to the lesser importance of the void in dc discharge plasmas, we leave its consideration out of the scope of our review and only provide the references to the existing, also rather extensive literature.[212,213,220,269–276]

The void appears if the CCRF discharge power exceeds a certain threshold, as it was observed in experiments[16,55] and reproduced in simulations.[69,218,219,277] The dependence of the void onset on the pressure is not clear. According to the simulations of PKE-Nefedov[63,69] and the experiments in PK-3 Plus setup,[55], the discharge power of the void onset is lower for lower discharge pressures. On the other hand, in the experiments with IMPF-KT chamber,[278] the void closure voltage increased with decreasing the gas pressure from 15 to 5 Pa. No significant dependence on the amount of the microparticles was revealed,[55,218,219,277] although increase of the amount of microparticles leads to the decrease of the void size. These experiments as well as the simulations showed that the void size grows with the increase of the discharge power. At certain discharge power, the void size can stabilize,[16,55,278] but with further power increase, it continues growing again.[55] The microparticle density experiences a maximum close to the void boundary.[16,55] The density peak disappears with the increase of the discharge power.

Thermophoretic force and IDF were considered to be responsible for the void formation. Both forces scale as a^2, which explains the void formation and growth in experiments with growing dust particles.[109,114,159,279] The role of possible attraction force between the microparticles was also discussed.[280,281] First estimations of the IDF by Morfill et al.[268] suggested that it is too small to compensate the electrostatic force. However, later it was shown by Khrapak et al. that the IDF was about an order of magnitude underestimated.[47] The results of void closure experiments by Lipaev et al.[16] were interpreted in terms of a single-particle approach, that is, the force balance was treated for a single microparticle immersed in the simulated field of dust-free plasma parameters. It demonstrated that the void can form due to the balance of electrostatic force and IDF. This idea, even nowadays, remains the baseline in the understanding of the physics of the void.

A group of experiments was dedicated to the measurement of forces acting on microparticles in the vicinity of the void boundary. In those experiments, the microparticles were injected into the void by a manipulation laser[282] or due to the trampoline effect (see Section 6.2.2).[283] The observation of the microparticles which fell through the void after the discharge power reduction,[284] were injected by a special accelerator,[285] or penetrated the void due to an unspecified reason[286] allowed to measure the force in the entire void volume. In each of these experiments, the results were reported for only a single set of conditions.

In early theoretical works, the stable void[287–289] as well as the void formation[290–293] were described based on 1D fluid equations. Neither rf-period-resolved electron dynamics nor external boundary of the suspension was considered. In some models,[291–293] even ionization and recombination on the microparticles were neglected.

To get better insight into microparticle–plasma interaction, the entire discharge was simulated.[63,65,66,68,69,215,217–219,277] The 1D fluid model by Gozadinos et al.[68] included both the absorption of plasma electrons and ions on the microparticles and the contribution of the microparticles to plasma quasineutrality. This model reproduced the appearance of the void with reducing the pressure and a peak of microparticle density at the void boundary.

The 2D fluid model[215,217–219,277] of PKE-Nefedov experiment demonstrated the increase of the electron energy in presence of the dust. The simulated void size was compared[218,219] with the experiment.[16] Although the model qualitatively reproduced the void formation and growth with increasing rf voltage, it predicted higher rf voltage of the void formation compared with that observed in the experiment. The coincidence with the experiment was achieved only by neglecting ion-neutral charge-exchange collisions. The "single-particle" void was shown to be larger and appear for lower powers than the void with the microparticle suspension effect considered. The electron density inside the void was much higher than inside the dust suspension (see Figure 12).

The early works were examined by comparing the dimensions and onset of the void formation in the simulations and the experiments without validation of the obtained background plasma conditions. Even the development of PIC codes[63,277] with a more thorough treatment of the electron kinetics did not lead to an immediate breakthrough. The first attempt[65] to compare the outcome of the PIC simulations with the microparticle arrangement and the rf PROES-measured spatiotemporal emission patterns in the experiment was unsuccessful in the sense of void problem, since in the simulations, "the sharp dust density gradients at the void edges resulted in unwanted boundary effects."

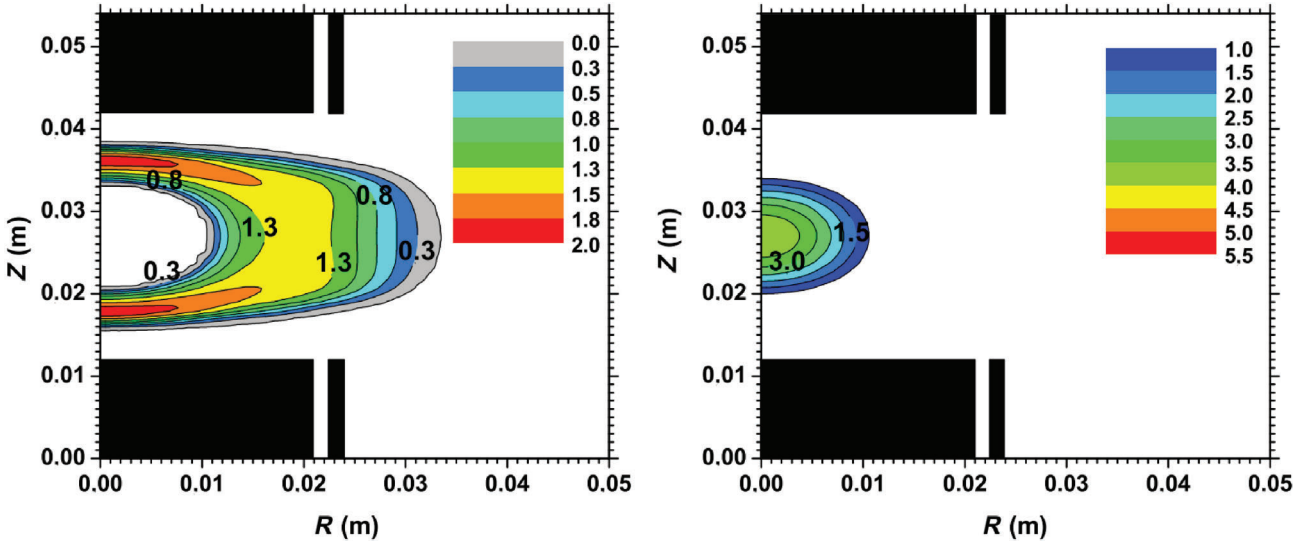

FIGURE 12 An example of the simulation results by Land and Goedheer.[217] Left: the dust density in 10^{10} m^{-3}. The dust-free void in the centre is clearly visible. Right: The electron density in 10^{15} m^{-3}. The electrons concentrate within the volume of the void

Another PIC model[66] was able to qualitatively reproduce the spatiotemporal emission pattern, but was unable to reproduce the formation of void. Imposing a fixed configuration of microparticles with a void in the simulation led to tremendous forces on the void boundaries and to the drastic distortion of the spatiotemporal emission pattern.

Results of the spectroscopic and probe investigations of the plasma conditions within the void were controversial. The electron energies in the void were qualitatively investigated using line-ratio method[147,294,295] and were found to be lower inside the void region compared with those inside the dust suspension. On the other hand, measurements with a Langmuir probe by Schulze et al.[234] revealed that both the electron temperature and density are higher inside the void than in the suspension. Klindworth et al.[132] performed Langmuir probe measurements under the microgravity conditions in a parabolic flight. In their experiment, the probe tip could be moved radially as well as axially. The measurements revealed axial and radial increase of electron temperature from the void towards the periphery of the suspension.

RF PROES measurements by Killer et al.[65] showed strong increase of the discharge emission in the centre of the discharge, where the void was located. However, the void in that experiment was so large that it was not clear if the emission was coupled with the void. Similar experiments by Pustylnik et al.[66] with varying the void position showed no void-related feature in the spatio-temporal emission patterns. In an experiment with growing (due to sputtering) dust particles,[121] a bright emission from the void was clearly visible. Similar feature was also present in the distribution of the resonance atoms measured with LIF. On the other hand, in an experiment with dust particles growing in an argon-acetylene mixture,[159] the plasma emission and the metastable density decreased during the void growth, and no local effects could be seen.

Investigation of this contradiction[55] showed that the void may exist in two regimes: "dim" and "bright." The dim void forms at relatively low discharge powers and exhibits no emission feature associated with it. After reaching a certain size, the dim void dimensions become almost independent on the discharge power. After the discharge power is increased to the threshold value, the void starts growing with the power increase again, and the bright emission from the void appears, that is, the void experiences a transition from dim to bright regime. With further discharge power increase, the plasma emission concentrates near the void boundaries, especially at higher gas pressure. The effect is demonstrated in Figure 13. RF PROES measurements revealed that the presence of the microparticles increases the emission in the entire axial extension of the discharge every half of the period in the case of the dim void, whereas for the bright void, the emission increase appears only between the expanding sheath and the opposite void boundary.

A simplified time-averaged 1D fluid model[55] could reproduce the bright void. The bright emission in the void was caused by the strong time-averaged electric field at the void boundary and elevated electron density inside the void. In this case, the void boundary stabilized as a result of the balance of IDF and electrostatic forces. This balance could only

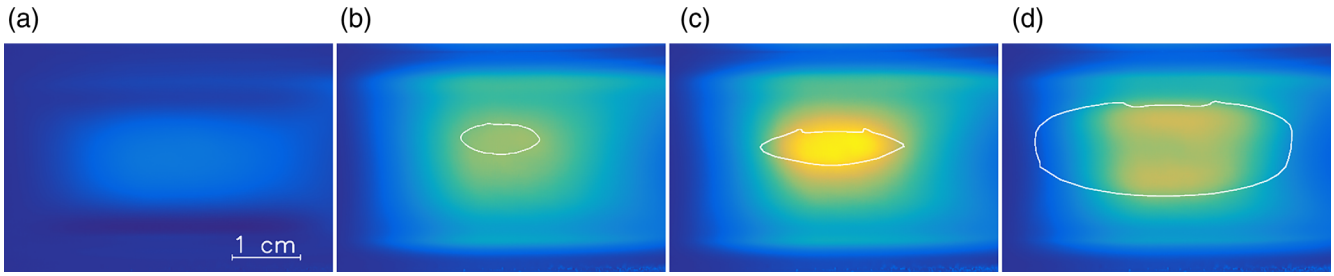

FIGURE 13 Colour-coded effect of the microparticles on the argon plasma emission in PK-3 Plus chamber. The emission is captured through a narrow-band spectral filter with the central wavelength of 750 nm. The plasma emission without the microparticles is subtracted. The white contours depict the void boundaries. The discharge power is about (a) 100, (b) 400, (c) 700, and (d) 1,200 mW. (a) No void; (b) the dim void; (c) the bright void; (d) the bright emission near the void boundaries. Details of the experiment are available in the paper by Pikalev et al.[55]

be satisfied at the elevated discharge power. The bright void was closing without the dim void phase with the decrease of the ionization rate as soon as the IDF was unable to balance the electrostatic force.

Dim void could be, however, obtained by artificially including the radial diffusion term into the ion flux continuity equation in a certain range of axial positions around the discharge midplane. Inside the microparticle suspension, the ionization balance was supposed to be local and therefore, the radial diffusion was neglected. Assuming radial diffusion rate to be comparable to the ionization and microparticle sink rates resulted in a microparticle-free region whose axial boundary was stabilized by the weak electrostatic forces. Electric field at the void boundary was in this case two orders of magnitude lower compared with that in the bright void regime and electron density distribution was flat. Such a low electric field did not lead to the appearance of the emission on the void boundary. The modified model was able to qualitatively explain the experimentally observed dim void formation as well as the respective experimentally measured rf-period-resolved spatiotemporal emission profile. At the same time, inclusion of the radial diffusion for the conditions of the bright void did not lead to qualitative changes. It was, therefore, demonstrated that the void in the dim and bright regimes forms due to two different mechanisms.

In addition to that, this model revealed that in the case of a dim void, the dc component of electric field vanished inside the dust suspension, whereas in the case of bright void, rather a strong ambipolar electric field existed inside the dust suspension. In the latter case, the balance between the electrostatic force and IDF was satisfied locally at every point of the suspension. This brings us back to the fundamental discussion on the principles of the self-organizations of dust suspensions immersed in plasmas initiated in Section 5.2.2. In the case of dim void, a dust suspension is formed according to the local ionization balance principle, whereas, in the case of bright void, the non-localities appear.

6.2.2 | Heartbeat instability

In the first microgravity experiments with complex plasmas, a spontaneous periodic contraction of the void boundary was reported.[296] Because of its characteristic appearance as well as due to very low repetition frequency (from single contractions to hundreds Hz), this phenomenon was termed “heartbeat” instability. The heartbeat instability was investigated under microgravity conditions on board the ISS,[17,297] in experiments with grown dust particles[298–301] and with the thermophoretic gravity compensation.[123,302] The self-excited heartbeat instability exists within a certain range of discharge power and gas pressure and requires relatively high density of the dust suspension.[123] The heartbeat self-excitation region in pressure—discharge power space is expanding with the increase of the amount of microparticles. At the lower discharge power boundary of the instability range, the void undergoes sporadic contractions with strong variation of the void size, while near the higher power boundary, the void size variation is decreasing with the increase of the discharge power, until the oscillations become undetectable.[302] The heartbeat frequencies depend on gas pressure, discharge power and size of the microparticles.[17,298]

The experiments showed that oscillations of the discharge electrical parameters and the plasma emission are inherent in the heartbeat instability. In the case of the instability with low repetition rate, when the void nearly restores between the contractions, the emission has a clear pattern (see Figure 14). Just before the void contraction, the plasma glow flashes

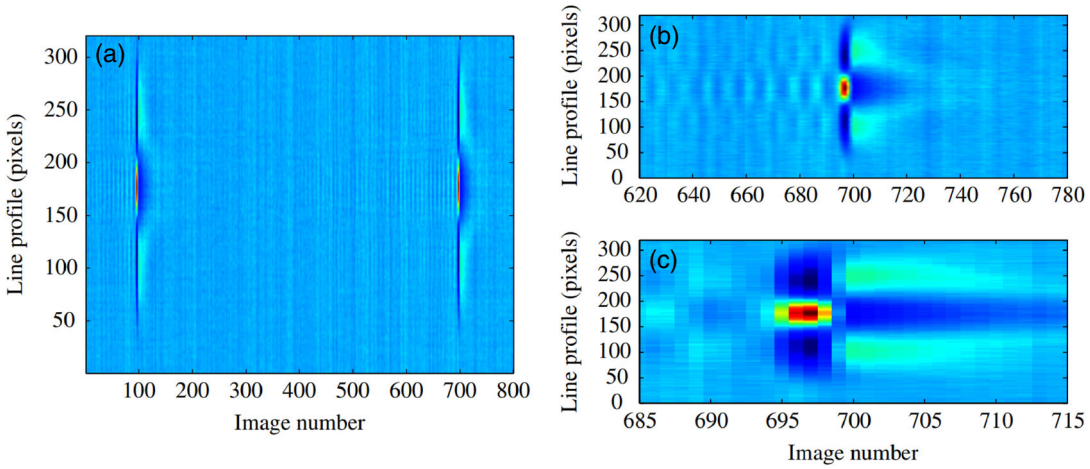

FIGURE 14 (a) Evolution of the plasma emission during the heartbeat instability (in false colours from dark blue to red). To construct this image, the horizontal line passing through the middle of the discharge is extracted from each video frame. A temporal average value is subtracted. The camera frame rate is 1,789 fps. (b) and (c) are different magnifications of (a). The figure is taken from the paper by Mikikian et al.[299]

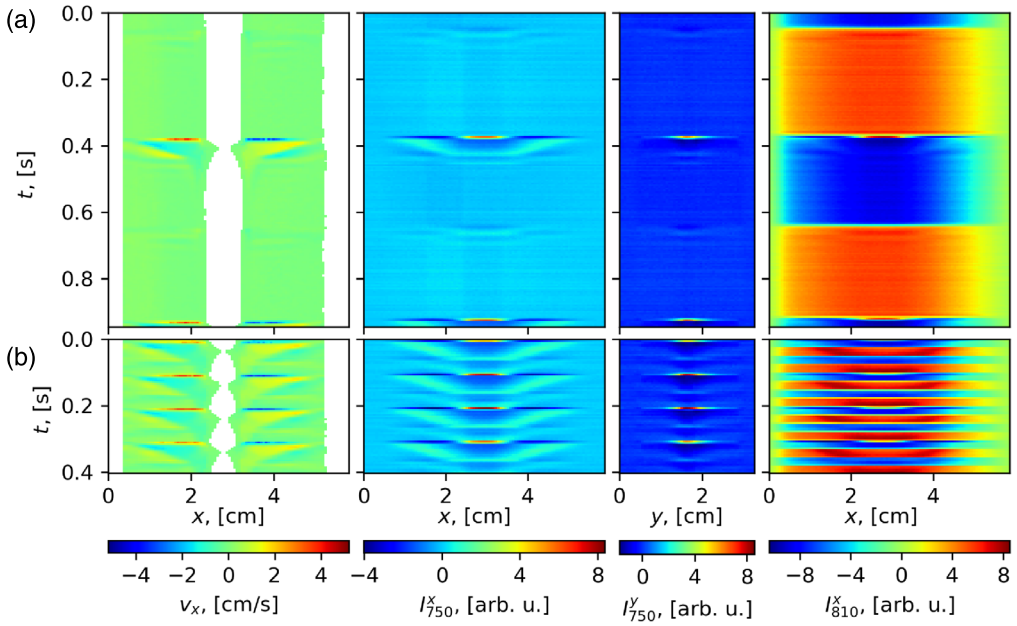

FIGURE 15 Transient optogalvanic excitation of the heartbeat instability. From the left to the right: velocities of the microparticles in the horizontal direction, horizontal and vertical distribution of the plasma emission variation captured through a narrow-band spectral filter with the central wavelength of 750 nm, horizontal distribution of the plasma emission variation (including laser-induced fluorescence signal) captured through a filter with the central wavelength of 810 nm. These patterns are constructed using values in horizontal and vertical bands passing through the void. A temporal average value of the emission is subtracted. The chopper frequency is (a) 1.7 Hz and (b) 19.6 Hz. Details of the experiment are available in the paper by Pikalev et al.[302]

along the discharge axis, especially in the void. The flash duration is several milliseconds. At the same time, the discharge edge regions become darker. After that, the emission decreases in the contracted void, whereas the emission from the edge regions increases above the level before the flash.[123,298,299,301,302] In other regimes, it is more difficult to match the flash with the microparticle motion.

The reported data on the variation of the electrical parameters are contradictory. The rf discharge current patterns for the growing dust particles could have qualitatively different shapes for different conditions.[298] In the experiments with grown dust particles[299] and low repetition rate, the flash was accompanied by a peak of the rf discharge current. For the

high repetition rate, there was also another sharp peak after the flash. In the microgravity experiments, the oscillations of the rf and dc currents as well as the rf voltage were also observed,[17,297] although low sampling rate could leave certain features unresolved.

Small oscillations of the microparticle motion, the plasma emission, and the rf current can occur between the heartbeat contractions.[299–303] They were termed also "failed contractions." Their growth before the flash corresponding to the void contraction is clearly visible in Figure 14. These oscillations seem to correspond to the radial breathing mode of the suspension.

The PTV was used to determine velocity and acceleration of the microparticles during the instability.[17,297] The particle tracing during the "trampoline effect" was used to determine the force distribution near the void boundary.[283] This effect is similar to the heartbeat instability. It involves, however, only a few microparticles that are pushed into the void.

The heartbeat instability is a source of waves[17,297] and turbulence.[12,304] The generated waves include low-frequency waves moving from the centre to the edge of the suspension, which were termed "oscillons."

The heartbeat instability can be controlled optogalvanically with a tunable laser. The effect was investigated with a diode laser tuned to the 772.38 nm spectral line of argon.[123,302] The effect was stronger when the laser beam passed through the void. The continuous laser beam stabilized the microparticle suspension. The laser beam modulated with a chopper could induce the heartbeat instability. If the laser power was high enough, the void contractions occurred transiently after each closing of the laser beam if the beam passed through the void (see Figure 15) or opening if the beam was shifted horizontally to the void edge. The modulated laser beam with low power could induce the instability resonantly, when the modulation frequency was close to the suspension (radial) breathing mode frequency.

The physical mechanism of the heartbeat instability is still unclear. According to rather a complicated static fluid theory of the void by Vladimirov et al.,[305] the void can acquire several stable or unstable configurations with different sizes. The heartbeat was supposed to be a transition between those configurations. A lot of simplifications and input parameters, which are difficult to evaluate experimentally, complicate the comparison of this model with the experiments. Another description of the heartbeat instability was based on an equivalent circuit model of the complex plasma.[297] The void oscillations were associated with the variation of the discharge capacitance.

The heartbeat instability was also supposed to occur due to a critical transformation on the void boundary.[123] Since the heartbeat instability is accompanied by the flash inside the void, it was suggested[302] that this critical transformation is nothing but an abrupt transition between the dim and bright void regimes (see Section 6.2.1). An increase of the ionization rate may switch the void from the dim to the bright regime.[55] The ionization rate can be modified by the laser which explains the optogalvanic control of the instability.[302] In the case of self-excited heartbeat instability, transition from the dim to the bright void regime is evidently mediated by the breathing oscillations, which serve as precursors of the heartbeat instability.[299,300,302]

Applying the concept of the two principles of the self-organization of the dust suspensions immersed in low-temperature plasma (formulated in Section 5.2.2) to the heartbeat instability, we may state that a suspension subjected to this instability "cannot decide" according to which principle it should self-organize.

7 | CONCLUSION

We have reviewed the state-of-the-art understanding of the phenomena of dust–plasma interactions. We limited our consideration to the two discharge types, namely to the dc discharge and the CCRF discharge. These two discharge types are mostly used in applications involving dust and are therefore best studied and understood.

Dust particles in low-temperature plasmas are subject to several basic processes. They collect charged species—electrons and ions—and, therefore, get charged; they exchange momentum with the charged and neutral components of the plasma and therefore become subject to ion drag and thermophoretic forces; they make a non-negligible contribution to the charge balance and therefore affect the electric fields in the plasma; they interact with each other by means of a screened Coulomb potential. Understanding of these basic processes allowed to construct the models of dusty discharges which, together with the application of modern diagnostic techniques in the experiments, drove the progress in the understanding of dust–plasma interactions in the last two decades.

The stable configuration of a dusty discharge has to satisfy the ionization balance, which unavoidably includes the collection of electrons and ions on the surfaces of dust particles, as well as the mechanical balance for the dust component, in which (in the absence of gravity) the electrostatic and IDFs usually dominate. In their models, Sukhinin et al.[211,212] and Fedoseev et al.[213] showed that this can be done in two different ways. In case of insufficient ionization

rate, the electrostatic force can only be compensated by ion drag in a trivial way, that is, when electric field vanishes. Ionization balance therefore localizes inside the dust suspension. In case of sufficiently high ionization rate, the detailed balance between the two forces may be provided, and the ionization balance remains non-local similarly to a dust-free discharge.

An important experimental manifestation of these two principles of the self-organization of dust suspensions in plasmas is the recently discovered existence of the two void regimes in a CCRF discharge.[55] The so-called "dim" void forms according to the first principle, whereas the so-called "bright" void forms according to the second principle. We note that the mechanical stability of the void boundary is provided by the commonly accepted principle of the balance of electrostatic and IDFs only in the case of bright void. The heartbeat instability appears to be nothing but the oscillation of the void between its dim and bright regimes.[302]

In spite of the obvious progress, the dust–plasma interactions are still very far from complete understanding. We have seen, for example, that explanation of the void required artificial introduction of the radial diffusion of ions in to the ion flux continuity equation. True two-dimensional model of the void in capacitively coupled discharge could reveal further features of the void formation, for example, explain the radial stability of the void. At the moment, such a model would be extremely computationally expensive and therefore very inconvenient for the research purposes. Simulations of dynamical multi-timescale phenomena (as, e.g., the heartbeat instability) are a way more challenging.

Also, further advances in plasma diagnostics are required to extend our knowledge of dust–plasma interactions. Measurement of ion velocity distributions is here of particular interest, since the ion velocities are in strong connection with the local electric field and also since the ions define the IDF—one of the two most important forces experienced by the dust particles. Extension of the LIF techniques of Arnas et al.[161,162] to higher pressures appears to be the most appropriate way.

We have seen how the usage of an imaging plasma diagnostic, namely, rf-period-resolved spectroscopy, lead to the progress in the understanding of the dust-induced excessive heating of electrons in CCRF plasmas.[64–66,151] There is no need to explain the advantage of imaging measurement techniques compared with line-averaged local measurements. Therefore, development of new diagnostics as two-dimensional imaging instruments would be a key to the future progress in the research of dust–plasma interactions. This is related to the above-mentioned measurements of the ion velocity distributions or, for example, to the LIF measurement of the temperatures of neutral atoms.

Calculations of the dust-induced effects on the neutral gas temperature field in plasmas lead to controversial results.[214–216,220] Laser-absorption measurements by Pikalev et al.[125] show only the evidence of dust-induced gas heating. Marshall et al.[157] showed that the LIF measurements suffer from problems with the laser power broadening and absorption of the laser light on its way through the plasma. Solution of these problems could help to directly measure the neutral gas temperature field in a plasma and make a further step in understanding of the dust-induced effects on it.

Experimental and numerical approaches used for the investigations of the void and the heartbeat instability could also be applied to the instabilities occurring during the dust growth such as filamentary mode,[147] void rotation,[222] carousel instability,[225] or the instability observed by Cavarroc et al.[231–233] as the low-frequency oscillations in the third harmonic of the rf current accompanied by the oscillations in the plasma emission intensity.

Microgravity complex plasma research became one of the drivers of the investigations of dust–plasma interactions during the last decade. Indeed, the phenomena discovered in the Plasmakristall-4 facility,[15] especially the so-called partitioning of the microparticle suspensions, cannot be explained by existing discharge models. The next-generation facility COMPACT[103] (formerly, EKoPlasma[104]), being a multi-electrode rf system with the possibility of rf pulsing and flexible geometry, will definitely add new computational and experimental challenges in the investigations of dust–plasma interactions.

ACKNOWLEDGEMENTS

The authors are thankful to Dr V. Nosenko for careful reading of the manuscript. The microgravity research is funded by the space administration of the Deutsches Zentrum für Luft- und Raumfahrt eV with funds from the Federal Ministry for Economy and Technology according to a resolution of the Deutscher Bundestag under Grants No. 50WM1441 and by the Bayerisches Staatsministerium für Wirtschaft und Medien, Energie und Technologie (StMWi). A. Pikalev acknowledges the financial support of Deutscher Akademischer Austauschdienst (DAAD) with funds from Deutsches Zentrum für Luft- und Raumfahrt e.V. (DLR). All authors greatly acknowledge the joint ESA-Roscosmos "Experiment Plasmakristall-4"

on-board the International Space Station. This work was also supported by the Ministry of Science and Higher Education of the Russian Federation (State Assignment No. 075-00460-21-00). Open Access funding enabled and organized by Projekt DEAL.

DATA AVAILABILITY STATEMENT

Data sharing is not applicable to this article as no new data were created or analyzed in this study.

REFERENCES

[1] National Academies of Sciences, Engineering and Medicine, Plasma Science: Enabling Technology, Sustainability, Security, and Exploration, The National Academies Press, Washington, DC **2021**.
[2] V. N. Tsytovich, *Physics-Uspekhi* **1997**, *40*(1), 53.
[3] S. V. Vladimirov, A. A. Samarian, K. Ostrikov, Physics and Applications of Complex Plasmas, London, Imperial College Press **2005**.
[4] U. R. Kortshagen, R. M. Sankaran, R. N. Pereira, S. L. Girshick, J. J. Wu, E. S. Aydil, *Chem. Rev.* **2016**, *116*(18), 11061.
[5] P. K. Shukla, A. A. Mamun, Introduction to Dusty Plasma Physics, Boca Raton, CRC Press **2001**.
[6] V. E. Fortov, A. G. Khrapak, S. A. Khrapak, V. I. Molotkov, O. F. Petrov, *Physics-Uspekhi* **2004**, *47*, 447.
[7] V. E. Fortov, G. E. Morfill, Complex and Dusty Plasmas, Boca Raton, CRC Press **2009**.
[8] C. R. Vandenabeele, S. Lucas, *Mater. Sci. Eng. R: Rep.* **2020**, *139*, 100521.
[9] G. E. Morfill, A. V. Ivlev, *Rev. Modern Phys.* **2009**, *81*, 1353.
[10] A. Ivlev, H. Löwen, G. Morfill, C. P. Royall, Complex Plasmas and Colloidal Dispersions: Particle-resolved Studies of Classical Liquids and Solids, Hackensack, World Scientific, **2012**.
[11] A. V. Ivlev, G. E. Morfill, H. M. Thomas, C. Räth, G. Joyce, P. Huber, R. Kompaneets, V. E. Fortov, A. M. Lipaev, V. I. Molotkov, T. Reiter, M. Turin, P. Vinogradov, *Phys. Rev. Lett.* **2008**, *100*, 095003.
[12] S. Zhdanov, M. Schwabe, C. Räth, H. M. Thomas, G. E. Morfill, *Europhys. Lett.* **2015**, *110*, 35001.
[13] A. P. Nefedov, G. E. Morfill, V. E. Fortov, H. M. Thomas, H. Rothermel, T. Hagl, A. V. Ivlev, M. Zuzic, B. A. Klumov, A. M. Lipaev, V. I. Molotkov, O. F. Petrov, Y. P. Gidzenko, S. K. Krikalev, W. Shepherd, A. I. Ivanov, M. Roth, H. Binnenbruck, J. A. Goree, Y. P. Semenov, *New J. Phys.* **2003**, *5*, 33.
[14] H. M. Thomas, G. E. Morfill, V. E. Fortov, A. V. Ivlev, V. I. Molotkov, A. M. Lipaev, T. Hagl, H. Rothermel, S. A. Khrapak, R. K. Sütterlin, M. Rubin-Zuzic, O. Petrov, V. I. Tokarev, S. K. Krikalev, *New J. Phys.* **2008**, *10*, 033036.
[15] M. Y. Pustylnik, M. A. Fink, V. Nosenko, T. Antonova, T. Hagl, H. M. Thomas, A. V. Zobnin, A. M. Lipaev, A. D. Usachev, V. I. Molotkov, O. F. Petrov, V. E. Fortov, C. Rau, C. Deysenroth, S. Albrecht, M. Kretschmer, M. H. Thoma, G. E. Morfill, R. Seurig, A. Stettner, A. Alyamovskaya, A. Orr, E. Kufner, E. G. Lavrenko, G. I. Padalka, E. O. Serova, A. M. Samokutyaev, S. Christoforetti, *Rev. Sci. Instrum.* **2016**, *87*, 093505.
[16] A. M. Lipaev, S. A. Khrapak, V. I. Molotkov, G. E. Morfill, V. E. Fortov, A. V. Ivlev, H. M. Thomas, A. G. Khrapak, V. N. Naumkin, A. I. Ivanov, S. E. Tretschev, G. I. Padalka, *Phys. Rev. Lett* **2007**, *98*, 265006.
[17] R. Heidemann, L. Couëdel, S. K. Zhdanov, R. K. Sütterlin, M. Schwabe, H. M. Thomas, A. V. Ivlev, T. Hagl, G. E. Morfill, V. E. Fortov, O. F. Petrov, A. M. Lipaev, V. Tokarev, T. Reiter, P. Vinogradov, *Phys. Plasmas* **2011**, *18*, 053701.
[18] A. V. Zobnin, A. D. Usachev, A. M. Lipaev, O. F. Petrov, V. E. Fortov, M. Yu Pustylnik, H. M. Thomas, M. A. Fink, M. H. Thoma, G. I. Padalka, *J. Phys. Conf. Ser.* **2016**, *774*, 012174.
[19] J. E. Allen, *Phys. Scr.* **1992**, *45*, 497.
[20] J. E. Allen, B. M. Annaratone, U. de Angelis, *J. Plasma Phys.* **2000**, *63*, 299.
[21] S. A. Khrapak, S. V. Ratynskaia, A. V. Zobnin, A. D. Usachev, V. V. Yaroshenko, M. H. Thoma, M. Kretschmer, H. Höfner, G. E. Morfill, O. F. Petrov, V. E. Fortov, *Phys. Rev. E* **2005**, *72*(1), 016406.
[22] L. G. D'yachkov, A. G. Khrapak, S. A. Khrapak, G. E. Morfill, *Phys. Plasmas* **2007**, *14*, 042102.
[23] A. V. Zobnin, A. D. Usachev, O. F. Petrov, V. E. Fortov, *Phys. Plasmas* **2008**, *15*, 043705.
[24] S. A. Khrapak, G. E. Morfill, *Phys. Plasmas* **2008**, *15*(11), 114503.
[25] A. V. Zobnin, A. P. Nefedov, V. A. Sinel'shchikov, V. E. Fortov, *J. Exp. Theor. Phys.* **2000**, *91*, 483.
[26] M. Lampe, R. Goswami, Z. Sternovsky, S. Robertson, V. Gavrishchaka, G. Ganguli, G. Joyce, *Phys. Plasmas* **2003**, *10*, 1500.
[27] I. H. Hutchinson, L. Patacchini, *Phys. Plasmas* **2007**, *14*(1), 013505.
[28] I. L. Semenov, A. G. Zagorodny, I. V. Krivtsun, *Phys. Plasmas* **2011**, *18*(10), 103707.
[29] I. L. Semenov, A. G. Zagorodny, I. V. Krivtsun, *Phys. Plasmas* **2012**, *19*, 043703.
[30] S. Ratynskaia, S. Khrapak, A. Zobnin, M. H. Thoma, M. Kretschmer, A. Usachev, V. Yaroshenko, R. A. Quinn, G. E. Morfill, O. Petrov, *Phys. Rev. Lett.* **2004**, *93*, 085001.
[31] O. Bystrenko, A. Zagorodny, *Phys. Rev. E* **2003**, *67*, 066403.
[32] S. A. Khrapak, G. E. Morfill, A. G. Khrapak, L. G. D'yachkov, *Phys. Plasmas* **2006**, *13*, 052114.
[33] T. Bystrenko, A. Zagorodny, *Phys. Lett. A* **2002**, *299*, 383.
[34] X.-Z. Tang, G. L. Delzanno, *Phys. Plasmas* **2014**, *21*(12), 123708.
[35] V. Nosenko, R. Fisher, R. Merlino, S. Khrapak, G. Morfill, K. Avinash, *Phys. Plasmas* **2007**, *14*(10), 103702.
[36] S. A. Khrapak, B. A. Klumov, G. E. Morfill, *Phys. Rev. Lett.* **2008**, *100*, 383.
[37] I. L. Semenov, S. A. Khrapak, H. M. Thomas, *Phys. Plasmas* **2015**, *22*, 053704.

[38] J. E. Daugherty, R. K. Porteous, M. D. Kilgore, D. B. Graves, *J. Appl. Phys.* **1992**, *72*, 3934.
[39] S. Ratynskaia, U. de Angelis, S. Khrapak, B. Klumov, G. E. Morfill, *Phys. Plasmas* **2006**, *13*(10), 104508.
[40] S. Khrapak, G. Morfill, *Contributions Plasma Phys.* **2009**, *49*, 148.
[41] R. Kompaneets, U. Konopka, A. V. Ivlev, V. Tsytovich, G. Morfill, *Phys. Plasmas* **2007**, *14*, 052108.
[42] P. Ludwig, W. J. Miloch, H. Kählert, M. Bonitz, *New J. Phys.* **2012**, *14*, 053016.
[43] R. Kompaneets, G. E. Morfill, A. V. Ivlev, *Phys. Rev. E* **2016**, *93*, 063201.
[44] I. H. Hutchinson, *Phys. Plasmas* **2011**, *18*, 032111.
[45] S. A. Khrapak, A. V. Ivlev, S. K. Zhdanov, G. E. Morfill, *Phys. Plasmas* **2005**, *12*, 042308.
[46] M. S. Barnes, J. H. Keller, J. C. Forster, J. A. O'Neill, D. K. Coultas, *Phys. Rev. Lett.* **1992**, *68*, 313.
[47] S. A. Khrapak, A. V. Ivlev, G. E. Morfill, H. M. Thomas, *Phys. Rev. E* **2002**, *66*, 046414.
[48] S. A. Khrapak, A. V. Ivlev, G. E. Morfill, S. K. Zhdanov, *Phys. Rev. Lett.* **2003**, *90*, 225002.
[49] I. L. Semenov, S. A. Khrapak, H. M. Thomas, *Phys. Plasmas* **2017**, *24*, 033710.
[50] S. A. Khrapak, *Phys. Plasmas* **2014**, *21*, 044506.
[51] L. Patacchini, I. H. Hutchinson, *Phys. Rev. Lett.* **2008**, *101*, 025001.
[52] I. H. Hutchinson, C. B. Haakonsen, *Phys. Plasmas* **2013**, *20*, 083701.
[53] I. L. Semenov, A. G. Zagorodny, I. V. Krivtsun, *Phys. Plasmas* **2013**, *20*(1), 013701.
[54] S. V. Vladimirov, S. A. Khrapak, M. Chaudhuri, G. E. Morfill, *Phys. Rev. Lett.* **2008**, *100*, 055002.
[55] A. Pikalev, I. Semenov, M. Pustylnik, C. Räth, H. Thomas, *Plasma Sources Sci. Technol.* **2021**, *30*, 035014.
[56] S. A. Khrapak, G. E. Morfill, *Phys. Rev. E* **2004**, *69*, 066411.
[57] D. Ticoş, A. Scurtu, J. D. Williams, L. Scott, E. Thomas, D. Sanford, C. M. Ticoş, *Phys. Rev. E* **2021**, *103*, 023210.
[58] P. S. Epstein, *Phys. Rev.* **1924**, *23*, 710.
[59] L. Talbot, R. K. Cheng, R. W. Schefer, D. R. Willis, *J. Fluid Mech.* **1980**, *101*, 737.
[60] G. H. P. M. Swinkels, H. Kersten, H. Deutsch, G. M. W. Kroesen, *J. Appl. Phys.* **2000**, *88*, 1747.
[61] F. Liu, K. J. Daun, D. R. Snelling, G. J. Smallwood, *Appl. Phys. B* **2006**, *83*, 355.
[62] S. A. Khrapak, G. E. Morfill, *Phys. Plasmas* **2006**, *13*(10), 104506.
[63] W. J. Goedheer, V. Land, J. Venema, *J. Phys. D: Appl. Phys.* **2009**, *42*(19), 194015.
[64] A. Melzer, S. Hübner, L. Lewerentz, K. Matyash, R. Schneider, R. Ikkurthi, *Phys. Rev. E* **2011**, *83*, 036411.
[65] C. Killer, G. Bandelow, K. Matyash, R. Schneider, A. Melzer, *Phys. Plasmas* **2013**, *20*, 083704.
[66] M. Y. Pustylnik, I. L. Semenov, E. Zähringer, H. M. Thomas, *Phys. Rev. E* **2017**, *96*, 033203.
[67] I. L. Semenov, *Phys. Rev. E* **2017**, *95*, 043208.
[68] G. Gozadinos, A. V. Ivlev, J. P. Boeuf, *New J. Phys.* **2003**, *5*, 32.
[69] V. Land, L. S. Matthews, T. W. Hyde, D. Bolser, *Phys. Rev. E* **2010**, *81*, 056402.
[70] M. M. Becker, H. Kählert, A. Sun, M. Bonitz, D. Loffhagen, *Plasma Sources Sci. Technol.* **2017**, *26*, 044001.
[71] A. D. Richards, B. E. Thompson, H. H. Sawin, *Appl. Phys. Lett.* **1987**, *50*, 492.
[72] J. P. Boeuf, *Phys. Rev. A* **1992**, *46*, 7910.
[73] P. Hartmann, M. Rosenberg, Z. Juhasz, L. S. Matthews, D. L. Sanford, K. Vermillion, J. C. Reyes, T. W. Hyde, *Plasma Sources Sci. Technol.* **2020**, *29*(11), 115014.
[74] T. Holstein, *Phys. Rev.* **1946**, *70*, 367.
[75] I. P. Shkarofsky, T.W. Johnston, M.P. Bachynski. The Particle Kinetics of Plasmas, Reading, Addison-Wesley, **1966**.
[76] R. A. Gottscho, A. Mitchell, G. R. Scheller, Y.-Y. Chan, D. B. Graves, *Phys. Rev. A* **1989**, *40*, 6407.
[77] V. I. Kolobov, L. D. Tsendin, *Phys. Rev. A* **1992**, *46*, 7837.
[78] D. N. Polyakov, V. V. Shumova, L. M. Vasilyak, V. E. Fortov, *Phys. Scr.* **2010**, *82*, 055501.
[79] L. M. Vasilyak, D. N. Polyakov, V. V. Shumova, *Contributions Plasma Phys.* **2013**, *53*, 432.
[80] D. N. Polyakov, V. V. Shumova, L. M. Vasilyak, *Surf. Eng. Appl. Electrochem.* **2013**, *49*, 114.
[81] V. V. Shumova, D. N. Polyakov, L. M. Vasilyak, *J. Phys. Conf. Ser.* **2015**, *653*, 012132.
[82] V. V. Shumova, D. N. Polyakov, L. M. Vasilyak, *Plasma Sources Sci. Technol.* **2017**, *26*, 035011.
[83] L. D. Tsendin, *Plasma Sources Sci. Technol.* **1995**, *4*, 200.
[84] G. I. Sukhinin, A. V. Fedoseev, *High Temp.* **2006**, *44*, 157.
[85] G. I. Sukhinin, A. V. Fedoseev, T. S. Ramazanov, K. N. Dzhumagulova, R. Z. Amangaliyeva, *J. Phys. D: Appl. Phys.* **2007**, *40*, 7761.
[86] G. I. Sukhinin, A. V. Fedoseev, *Phys. Rev. E* **2010**, *81*(1), 016402.
[87] A. V. Zobnin, A. D. Usachev, O. F. Petrov, V. E. Fortov, M. H. Thoma, M. A. Fink, *Phys. Plasmas* **2018**, *25*, 033702.
[88] Y. P. Raizer, Gas Discharge Physics, Springer-Verlag, Berlin Heidelberg **1991**.
[89] V. E. Fortov, A. P. Nefedov, V. M. Torchinskii, V. I. Molotkov, A. G. Khrapak, O. F. Petrov, K. F. Volykhin, *J. Exp. Theor. Phys. Lett.* **1996**, *64*, 92.
[90] V. I. Molotkov, O. F. Petrov, M. Y. Pustyl'nik, V. M. Torchinskii, V. E. Fortov, A. G. Khrapak, *High Temp.* **2004**, *42*, 827.
[91] D. N. Polyakov, V. V. Shumova, L. M. Vasilyak, *Plasma Phys. Rep.* **2017**, *43*, 397.
[92] P. S. Landa, N. A. Miskinova, Y. V. Ponomarev, *Soviet Phys. Uspekhi* **1980**, *23*(12), 813.
[93] A. P. Nefedov, O. S. Vaulina, O. F. Petrov, V. I. Molotkov, V. M. Torchinskiĭ, V. E. Fortov, A. V. Chernyshev, A. M. Lipaev, A. I. Ivanov, A. Y. Kaleri, Y. P. Semenov, S. V. Zaletin, *JETP* **2002**, *95*, 673.

[94] A. P. Nefedov, O. S. Vaulina, O. F. Petrov, V. I. Molotkov, V. M. Torchinskii, V. E. Fortov, A. V. Chernyshev, A. M. Lipaev, A. I. Ivanov, A. Y. Kaleri, Y. P. Semenov, S. V. Zaletin, *New J. Phys* **2003**, *5*, 108.
[95] V. E. Fortov, G. E. Morfill, O. Petrov, M. H. Thoma, A. D. Usachev, H. Höfner, A. V. Zobnin, M. Kretschmer, S. Ratynskaya, M. A. Fink, K. Tarantik, Y. Gerasimov, V. Esenkov, *Plasma Phys. Control. Fusion* **2005**, *47*, B537.
[96] M. H. Thoma, M. A. Fink, H. Höfner, M. Kretschmer, S. A. Khrapak, S. Ratynskaya, V. V. Yaroshenko, G. E. Morfill, O. F. Petrov, A. D. Usachev, A. V. Zobnin, V. E. Fortov, *IEEE Trans. Plasma Sci.* **2007**, *35*, 255.
[97] M. A. Fink, M. H. Thoma, G. E. Morfill, *Microgravity Sci. Technol.* **2011**, *23*, 169.
[98] Y. P. Raizer, M. N. Shneider, N. A. Yatsenko, Radio-Frequency Capacitive Discharges, Boca Raton, CRC Press **1995**.
[99] C. Bohm, J. Perrin, *J. Phys. D: Appl. Phys.* **1991**, *24*, 865.
[100] K. Tachibana, Y. Hayashi, T. Okuno, T. Tatsuta, *Plasma Sources Sci. Technol.* **1994**, *3*, 314.
[101] A. Bouchoule, A. Plain, L. Boufendi, J. P. Blondeau, C. Laure, *J. Appl. Phys.* **1991**, *70*, 1991.
[102] P. J. Hargis, K. E. Greenberg, P. A. Miller, J. B. Gerardo, J. R. Torczynski, M. E. Riley, G. A. Hebner, J. R. Roberts, J. K. Olthoff, J. R. Whetstone, R. J. Van Brunt, M. A. Sobolewski, H. M. Anderson, M. P. Splichal, J. L. Mock, P. Bletzinger, A. Garscadden, R. A. Gottscho, G. Selwyn, M. Dalvie, J. E. Heidenreich, J. W. Butterbaugh, M. L. Brake, M. L. Passow, J. Pender, A. Lujan, M. E. Elta, D. B. Graves, H. H. Sawin, M. J. Kushner, J. T. Verdeyen, R. Horwath, T. R. Turner, *Rev. Sci. Instrum.* **1994**, *65*, 140.
[103] C. A. Knapek, U. Konopka, D. P. Mohr, P. Huber, A. Lipaev, H. M. Thomas, *Rev. Sci. Instrum.* **2021**.
[104] C. A. Knapek, P. Huber, D. P. Mohr, E. Zaehringer, V. I. Molotkov, A. M. Lipaev, V. Naumkin, U. Konopka, H. M. Thomas, V. E. Fortov, *AIP Conf. Proc.* **2018**, *1925*, 020004.
[105] S. Mitic, M. Y. Pustylnik, E. Kovačević, J. Berndt, L. Boufendi, G. E. Morfill, *J. Phys. D: Appl. Phys.* **2012**, *45*, 335203.
[106] V. Y. Karasev, V. A. Polishchyuk, A. P. Gorbenko, E. S. Dzlieva, M. A. Ermolenko, M. M. Makar, *Phys. Solid State* **2016**, *58*, 1041.
[107] P. Belenguer, J. P. Blondeau, L. Boufendi, M. Toogood, A. Plain, A. Bouchoule, C. Laure, J. P. Boeuf, *Phys. Rev. A* **1992**, *46*(12), 7923.
[108] L. Boufendi, A. Bouchoule, *Plasma Sources Sci. Technol.* **1994**, *3*, 262.
[109] S. Hong, J. Berndt, J. Winter, *Plasma Sources Sci. Technol.* **2002**, *12*(1), 46.
[110] J.-C. Schauer, S. Hong, J. Winter, *Plasma Sources Sci. Technol.* **2004**, *13*, 636.
[111] I. Stefanovic, C. Scharwitz, E. Kovacevic, J. Berndt, J. Winter, *IEEE Trans. Plasma Sci.* **2008**, *36*, 1018.
[112] S. Mitic, M. Y. Pustylnik, G. E. Morfill, E. Kovačević, *Optics Lett.* **2011**, *36*(18), 3699.
[113] F. M. J. H. van de Wetering, J. Beckers, G. M. W. Kroesen, *J. Phys. D: Appl. Phys.* **2012**, *45*, 485205.
[114] F. M. J. H. Van de Wetering, R. J. C. Brooimans, S. Nijdam, J. Beckers, G. M. W. Kroesen, *J. Phys. D: Appl. Phys* **2015**, *48*, 035204.
[115] V. I. Molotkov, A. P. Nefedov, M. Y. Pustyl'nik, V. M. Torchinsky, V. E. Fortov, A. G. Khrapak, K. Yoshino, *J. Exp. Theor. Phys. Lett.* **2000**, *71*, 102.
[116] B. M. Annaratone, A. G. Khrapak, A. V. Ivlev, G. Söllner, P. Bryant, R. Sütterlin, U. Konopka, K. Yoshino, M. Zuzic, H. M. Thomas, G. E. Morfill, *Phys. Rev. E* **2001**, *63*, 036406.
[117] M. Y. Pustylnik, N. Ohno, S. Takamura, R. Smirnov, *Phys. Rev. E* **2006**, *74*, 046402.
[118] F. Wieben, D. Block, *Phys. Plasmas* **2018**, *25*(12), 123705.
[119] F. Wieben, D. Block, *Phys. Rev. Lett.* **2019**, *123*, 225001.
[120] M. Mikikian, L. Boufendi, A. Bouchoule, H. M. Thomas, G. E. Morfill, A. P. Nefedov, V. E. Fortov, the PKE-Nefedov team, *New J. Phys.* **2003**, *5*, 19.
[121] H. Tawidian, F. Diop, T. Lecas, T. Gibert, M. Mikikian, 40th EPS Conf. Plasma Phys, Espoo, Finland, **2013**, P1.304. http://ocs.ciemat.es/EPS2013PAP/pdf/P1.304.pdf.
[122] H. Rothermel, T. Hagl, G. E. Morfill, M. H. Thoma, H. M. Thomas, *Phys. Rev. Lett.* **2002**, *89*, 175001.
[123] M. Y. Pustylnik, A. V. Ivlev, N. Sadeghi, R. Heidemann, S. Mitic, H. M. Thomas, G. E. Morfill, *Phys. Plasmas* **2012**, *19*(10), 103701.
[124] C. Killer, M. Mulsow, A. Melzer, *Plasma Sources Sci. Technol.* **2015**, *24*, 025029.
[125] A. Pikalev, M. Pustylnik, C. Räth, H. Thomas, *J. Phys. D: Appl. Phys.* **2020**, *53*, 075203.
[126] D. N. Polyakov, V. V. Shumova, L. M. Vasilyak, V. E. Fortov, *Phys. Lett. A* **2011**, *375*, 3300.
[127] M. A. Sobolewski, *J. Vac. Sci. Technol. A: Vac. Surfaces Films* **1992**, *10*, 3550.
[128] L. Boufendi, J. Gaudin, S. Huet, G. Viera, M. Dudemaine, *Appl. Phys. Lett.* **2001**, *79*, 4301.
[129] G. Wattieaux, A. Mezeghrane, L. Boufendi, *Phys. Plasmas* **2011**, *18*, 093701.
[130] M. Henault, G. Wattieaux, T. Lecas, J. P. Renouard, L. Boufendi, *Phys. Plasmas* **2016**, *23*, 023504.
[131] V. A. Godyak, V. I. Demidov, *J. Phys. D: Appl. Phys.* **2011**, *44*, 269501.
[132] M. Klindworth, O. Arp, A. Piel, *Rev. Sci. Instrum.* **2007**, *78*, 033502.
[133] N. Bilik, R. Anthony, B. A. Merritt, E. S. Aydil, U. R. Kortshagen, *J. Phys. D: Appl. Phys.* **2015**, *48*(10), 105204.
[134] M. Klindworth, A. Piel, A. Melzer, U. Konopka, H. Rothermel, K. Tarantik, G. E. Morfill, *Phys. Rev. Lett.* **2004**, *93*(19), 195002.
[135] Sorokin, M, PhD Thesis, Dust Particle Formation in Silane Plasmas, **2005**. https://research.tue.nl/en/publications/dust-particle-formation-in-silane-plasmas(27f72ecb-19bc-4df1-bc92-3fe5103a3f3c).html.
[136] J. Berndt, E. Kovačević, V. Selenin, I. Stefanović, J. Winter, *Plasma Sources Sci. Technol.* **2005**, *15*(1), 18.
[137] C. Killer, T. Wegner, A. Melzer, J. Meichsner, *Phys. Plasmas* **2015**, *22*(12), 123702.
[138] I. A. Vasil'eva, *Physics-Uspekhi* **1993**, *36*, 694.
[139] I. A. Vasil'eva, *Physics-Uspekhi* **2001**, *44*(12), 1255.
[140] V. N. Ochkin, Spectroscopy of Low Temperature Plasma, Weinheim, Wiley **2009**.

[141] X.-M. Zhu, Y.-K. Pu, *J. Phys. D: Appl. Phys.* **2009**, *43*(1), 015204.
[142] B. John, R. O. J. Boffard, C. C. Lin, A. E. Wendt, *Plasma Sources Sci. Technol.* **2010**, *19*, 065001.
[143] X.-M. Zhu, P. Yi-Kang, Y. Celik, S. Siepa, E. Schüngel, D. Luggenhölscher, U. Czarnetzki, *Plasma Sources Sci. Technol.* **2012**, *21*, 024003.
[144] S. Mitic, J. Kaupe, P. Riedl, D. Coenen, *Phys. Plasmas* **2019**, *26*, 073507.
[145] A. Bouchoule, L. Boufendi, *Plasma Sources Sci. Technol.* **1993**, *2*, 204.
[146] A. Pikalev, V. Kobylin, A. Semenov, *IEEE Trans. Plasma Sci.* **2018**, *46*, 698.
[147] D. Samsonov, J. Goree, *Phys. Rev. E* **1999**, *59*(1), 1047.
[148] M. Schulze, A. Yanguas-Gil, A. von Keudell, P. Awakowicz, *J. Phys. D: Appl. Phys.* **2008**, *41*, 065206.
[149] V. Sushkov, A.-P. Herrendorf, R. Hippler, *J. Phys. D: Appl. Phys.* **2016**, *49*, 425201.
[150] T. Gans, V. Schulz von der Gathen, H. F. Döbele, *Contributions Plasma Phys.* **2004**, *44*, 523.
[151] S. Hübner, A. Melzer, *Phys. Rev. Lett.* **2009**, *102*, 215001.
[152] R. A. Stern, J. A. Johnson, *Phys. Rev. Lett.* **1975**, *34*, 1548.
[153] N. I. Uzelac, F. Leisf, *Spectrochim. Acta Part B: Atomic Spectrosc.* **1992**, *47*, 877.
[154] A. M. Keesee, E. E. Scime, R. F. Boivin, *Rev. Sci. Instrum.* **2004**, *75*(10), 4091.
[155] H. T. Do, H. Kersten, R. Hippler, *New J. Phys.* **2008**, *10*, 053010.
[156] M. J. Goeckner, J. Goree, *J. Vac. Sci. Technol. A: Vac. Surfaces Films* **1989**, *7*, 977.
[157] R. S. Marshall, P. M. Bellan, *Rev. Sci. Instrum.* **2020**, *91*, 063504.
[158] H. T. Do, V. Sushkov, R. Hippler, *New J. Phys.* **2009**, *11*, 033020.
[159] I. Stefanović, N. Sadeghi, J. Winter, B. Sikimić, *Plasma Sources Sci. Technol.* **2017**, *26*, 065014.
[160] G. D. Severn, D. A. Edrich, R. McWilliams, *Rev. Sci. Instrum.* **1998**, *69*(1), 10.
[161] C. Arnas, M. Mikikian, G. Bachet, F. Doveil, *Phys. Plasmas* **2000**, *7*(11), 4418.
[162] C. Arnas, M. Mikikian, F. Doveil, *Phys. Scr.* **2001**, *T89*(1), 163.
[163] J. E. M. Goldsmith, J. E. Lawler, *Contemp. Phys.* **1981**, *22*, 235.
[164] B. Barbieri, N. Beverini, A. Sasso, *Rev. Modern Phys.* **1990**, *62*, 603.
[165] J. Berndt, S. Hong, E. Kovačević, I. Stefanović, J. Winter, *Vacuum* **2003**, *71*, 377.
[166] F. R. A. Onofri, M. Wozniak, S. Barbosa, *Contributions Plasma Phys.* **2011**, *51*, 228.
[167] F. Kirchschlager, S. Wolf, F. Greiner, S. Groth, A. Labdon, *Appl. Phys. Lett.* **2017**, *110*(17), 173106.
[168] C. Pattyn, E. Kovacevic, S. Hussain, A. Dias, T. Lecas, J. Berndt, *Appl. Phys. Lett.* **2018**, *112*(1), 013102.
[169] N. Kohlmann, F. Wieben, O. H. Asnaz, D. Block, F. Greiner, *Phys. Plasmas* **2019**, *26*, 053701.
[170] M. Himpel, C. Killer, B. Buttenschön, A. Melzer, *Phys. Plasmas* **2012**, *19*(12), 123704.
[171] Y. Feng, J. Goree, Z. Haralson, C.-S. Wong, A. Kananovich, W. Li, *J. Plasma Phys.* **2016**, *82*, 615820303.
[172] J. D. Williams, *J. Plasma Phys.* **2016**, *82*, 615820302.
[173] T. Trottenberg, A. Melzer, A. Piel, *Plasma Sources Sci. Technol.* **1995**, *4*, 450.
[174] V. E. Fortov, A. P. Nefedov, V. I. Molotkov, M. Y. Poustylnik, V. M. Torchinsky, *Phys. Rev. Lett.* **2001**, *87*, 205002.
[175] V. E. Fortov, O. F. Petrov, A. D. Usachev, A. V. Zobnin, *Phys. Rev. E* **2004**, *70*, 046415.
[176] V. Nosenko, J. Meyer, S. K. Zhdanov, H. M. Thomas, *AIP Adv.* **2018**, *8*(12), 125303.
[177] T. Antonova, S. A. Khrapak, M. Y. Pustylnik, M. Rubin-Zuzic, H. M. Thomas, A. M. Lipaev, A. D. Usachev, V. I. Molotkov, M. H. Thoma, *Phys. Plasmas* **2019**, *26*(11), 113703.
[178] Y. Feng, J. Goree, B. Liu, *Rev. Sci. Instrum.* **2007**, *78*, 053704.
[179] Y. Ivanov, A. Melzer, *Rev. Sci. Instrum.* **2007**, *78*, 033506.
[180] Y. Feng, J. Goree, B. Liu, *Rev. Sci. Instrum.* **2011**, *82*, 053707.
[181] I. Grant, *Proc. Inst. Mech. Eng. Part C: J. Mech. Eng. Sci.* **1997**, *211*(1), 55.
[182] E. Thomas, M. Watson, *Phys. Plasmas* **1999**, *6*(10), 4111.
[183] E. Thomas, J. D. Williams, J. Silver, *Phys. Plasmas* **2004**, *11*, L37.
[184] J. D. Williams, *Phys. Plasmas* **2011**, *18*, 050702.
[185] J. D. Williams, E. Thomas, L. Couëdel, A. V. Ivlev, S. K. Zhdanov, V. Nosenko, H. M. Thomas, G. E. Morfill, *Phys. Rev. E* **2012**, *86*, 046401.
[186] A. D. Usachev, A. V. Zobnin, O. F. Petrov, V. E. Fortov, M. H. Thoma, M. Y. Pustylnik, M. A. Fink, G. E. Morfill, *Plasma Sources Sci. Technol.* **2016**, *25*, 035009.
[187] M. Y. Pustylnik, B. Klumov, M. Rubin-Zuzic, A. M. Lipaev, V. Nosenko, D. Erdle, A. D. Usachev, A. V. Zobnin, V. I. Molotkov, G. Joyce, H. M. Thomas, M. H. Thoma, O. F. Petrov, V. E. Fortov, O. Kononenko, *Phys. Rev. Res.* **2020**, *2*, 033314.
[188] S. Mitic, M. Y. Pustylnik, D. Erdle, A. M. Lipaev, A. D. Usachev, A. V. Zobnin, M. H. Thoma, H. M. Thomas, O. F. Petrov, V. E. Fortov, O. Kononenko, *Phys. Rev. E* **2021**, *103*, 063212.
[189] M. Jambor, V. Nosenko, S. K. Zhdanov, H. M. Thomas, *Rev. Sci. Instrum.* **2016**, *87*, 033505.
[190] M. Kroll, S. Harms, D. Block, A. Piel, *Phys. Plasmas* **2008**, *15*, 063703.
[191] S. Käding, A. Melzer, *Phys. Plasmas* **2006**, *13*, 090701.
[192] A. Melzer, M. Himpel, H. Krüger, M. Mulsow, S. Schütt, *Plasma Phys. Control. Fusion* **2018**, *61*(1), 014029.
[193] V. E. Fortov, A. D. Usachev, A. V. Zobnin, V. I. Molotkov, O. F. Petrov, *Phys. Plasmas* **2003**, *10*, 1199.

[194] S. Jaiswal, M. Y. Pustylnik, S. Zhdanov, H. M. Thomas, A. M. Lipaev, A. D. Usachev, V. I. Molotkov, V. E. Fortov, M. H. Thoma, O. V. Novitskii, *Phys. Plasmas* **2018**, *25*, 083705.
[195] R. L. Heinisch, F. X. Bronold, H. Fehske, *Phys. Rev. Lett.* **2012**, *109*, 243903.
[196] R. L. Heinisch, F. X. Bronold, H. Fehske, *Phys. Rev. E* **2013**, *88*, 023109.
[197] S. V. Vladimirov, O. Ishihara, *Phys. Rev. E* **2016**, *94*(1), 013202.
[198] S. V. Vladimirov, O. Ishihara, *Adv. Phys. X* **2017**, *2*, 462.
[199] H. Krüger, C. Killer, S. Schütt, A. Melzer, *Plasma Sources Sci. Technol.* **2018**, *27*, 025004.
[200] K. Dimoff, P. R. Smy, *Phys. Lett. A* **1970**, *32*(1), 13.
[201] S. Mitic, M. Y. Pustylnik, G. E. Morfill, *New J. Phys* **2009**, *11*, 083020.
[202] J. Schulze, A. Derzsi, K. Dittmann, T. Hemke, J. Meichsner, Z. Donkó, *Phys. Rev. Lett.* **2011**, *107*, 275001.
[203] T. Hemke, D. Eremin, T. Mussenbrock, A. Derzsi, Z. Donkó, K. Dittmann, J. Meichsner, J. Schulze, *Plasma Sources Sci. Technol.* **2012**, *22*(1), 015012.
[204] E. Schüngel, S. Mohr, S. Iwashita, J. Schulze, U. Czarnetzki, *J. Phys. D: Appl. Phys.* **2013**, *46*(17), 175205.
[205] A. A. Fridman, L. Boufendi, T. Hbid, B. V. Potapkin, A. Bouchoule, *J. Appl. Phys.* **1996**, *79*, 1303.
[206] Z. Shen, U. Kortshagen, *J. Vac. Sci. Technol. A: Vac. Surfaces Films* **2002**, *20*(1), 153.
[207] I. Denysenko, J. Berndt, E. Kovacevic, I. Stefanovic, V. Selenin, J. Winter, *Phys. Plasmas* **2006**, *13*, 073507.
[208] I. Stefanović, N. Sadeghi, J. Winter, *J. Phys. D: Appl. Phys.* **2010**, *43*(15), 152003.
[209] A. D. Usachev, A. V. Zobnin, A. V. Shonenkov, A. M. Lipaev, V. I. Molotkov, O. F. Petrov, V. E. Fortov, M. Y. Pustyl'nik, M. A. Fink, M. A. Thoma, H. M. Thomas, G. I. Padalka, *J. Phys. Conf. Ser.* **2018**, *946*, 012143.
[210] M. A. Lieberman, A. J. Lichtenberg, Principles of Plasma Discharges and Materials Processing. Hoboken, John Wiley & Sons, Inc **2005**.
[211] G. I. Sukhinin, A. V. Fedoseev, S. N. Antipov, O. F. Petrov, V. E. Fortov, *Phys. Rev. E* **2013**, *87*(1), 013101.
[212] G. I. Sukhinin, A. V. Fedoseev, M. V. Salnikov, S. N. Antipov, O. F. Petrov, V. E. Fortov, *Europhys. Lett.* **2013**, *103*, 35001.
[213] A. V. Fedoseev, G. I. Sukhinin, M. K. Dosbolayev, T. S. Ramazanov, *Phys. Rev. E* **2015**, *92*, 023106.
[214] J. Perrin, P. Molinas-Mata, P. Belenguer, *J. Phys. D: Appl. Phys.* **1994**, *27*(12), 2499.
[215] M. R. Akdim, W. J. Goedheer, *Phys. Rev. E* **2003**, *67*, 066407.
[216] M. R. Akdim, W. J. Goedheer, *Phys. Rev. E* **2003**, *67*, 056405.
[217] V. Land, W. J. Goedheer, *New J. Phys.* **2007**, *9*, 246.
[218] W. J. Goedheer, V. Land, *Plasma Phys. Control. Fusion* **2008**, *50*(12), 124022.
[219] V. Land, W. J. Goedheer, *New J. Phys.* **2008**, *10*(12), 123028.
[220] D. N. Polyakov, V. V. Shumova, L. M. Vasilyak, *Digest J. Nanomater. Biostructures* **2014**, *9*(12), 1249.
[221] V. V. Zhakhovskii, V. I. Molotkov, A. P. Nefedov, V. M. Torchinskii, A. G. Khrapak, V. E. Fortov, *J. Exp. Theor. Phys. Lett.* **1997**, *66*, 419.
[222] G. Praburam, J. Goree, *Phys. Plasmas* **1996**, *3*, 1212.
[223] M. Mikikian, M. Cavarroc, L. Couëdel, L. Boufendi, *Phys. Plasmas* **2006**, *13*, 092103.
[224] M. Mikikian, L. Couëdel, M. Cavarroc, Y. Tessier, L. Boufendi, *IEEE Trans. Plasma Sci.* **2008**, *36*, 1012.
[225] M. Mikikian, L. Couedel, Y. Tessier, L. Boufendi, *IEEE Trans. Plasma Sci.* **2011**, *39*(11), 2748.
[226] M. Mikikian, H. Tawidian, T. Lecas, *Phys. Rev. Lett.* **2012**, *109*, 245007.
[227] H. Tawidian, T. Lecas, M. Mikikian, *IEEE Trans. Plasma Sci.* **2013**, *41*, 754.
[228] H. Tawidian, T. Lecas, M. Mikikian, 40th EPS Conf. Plasma Phys, Espoo, Finland, **2013**, O5.311. http://ocs.ciemat.es/EPS2013PAP/pdf/O5.311.pdf.
[229] H. Tawidian, T. Lecas, M. Mikikian, *Plasma Sources Sci. Technol.* **2014**, *23*, 065009.
[230] J. F. Lagrange, I. Géraud-Grenier, F. Faubert, V. Massereau-Guilbaud, *J. Appl. Phys.* **2015**, *118*(16), 163302.
[231] M. Cavarroc, M. C. Jouanny, K. Radouane, M. Mikikian, L. Boufendi, *J. Appl. Phys.* **2006**, *99*, 064301.
[232] M. Cavarroc, M. Mikikian, G. Perrier, L. Boufendi, *Appl. Phys. Lett.* **2006**, *89*(1), 013107.
[233] M. Cavarroc, M. Mikikian, Y. Tessier, L. Boufendi, *Phys. Plasmas* **2008**, *15*(10), 103704.
[234] M. Schulze, A. von Keudell, P. Awakowicz, *Plasma Sources Sci. Technol.* **2006**, *15*, 556.
[235] M. Schulze, D. O'Connell, T. Gans, P. Awakowicz, A. von Keudell, *Plasma Sources Sci. Technol.* **2007**, *16*, 774.
[236] R. L. Merlino, *J. Plasma Phys.* **2014**, *80*, 773.
[237] J. H. Chu, J.-B. Du, I. Lin, *J. Phys. D: Appl. Phys.* **1994**, *27*, 296.
[238] N. D'Angelo, *J. Phys. D: Appl. Phys.* **1995**, *28*, 1009.
[239] A. Barkan, R. L. Merlino, N. D'Angelo, *Phys. Plasmas* **1995**, *2*(10), 3563.
[240] V. I. Molotkov, A. P. Nefedov, V. M. Torchinskii, V. E. Fortov, A. G. Khrapak, *J. Exp. Theor. Phys.* **1999**, *89*, 477.
[241] E. Thomas, *Phys. Plasmas* **2006**, *13*, 042107.
[242] J. Goree, B. Liu, M. Y. Pustylnik, H. M. Thomas, V. E. Fortov, A. M. Lipaev, V. I. Molotkov, A. D. Usachev, O. F. Petrov, M. H. Thoma, E. Thomas, U. Konopka, S. Prokopiev, *Phys. Plasmas* **2020**, *27*(12), 123701.
[243] A. Piel, O. Arp, M. Klindworth, A. Melzer, *Phys. Rev. E* **2008**, *77*, 026407.
[244] M. Schwabe, M. Rubin-Zuzic, S. Zhdanov, H. M. Thomas, G. E. Morfill, *Phys. Rev. Lett.* **2007**, *99*, 095002.
[245] K. O. Menzel, O. Arp, A. Piel, *Phys. Rev. Lett.* **2010**, *104*, 235002.
[246] V. Nosenko, S. K. Zhdanov, S.-H. Kim, J. Heinrich, R. L. Merlino, G. E. Morfill, *Europhys. Lett.* **2009**, *88*, 65001.

[247] U. Kortshagen, *Appl. Phys. Lett.* **1997**, *71*, 208.
[248] F. Melandsø, T. K. Aslaksen, O. Havnes, *J. Geophys. Res. Space Phys.* **1993**, *98*, 13315.
[249] M. Rosenberg, *Planet. Space Sci.* **1993**, *41*, 229.
[250] M. Rosenberg, *J. Vac. Sci. Technol. A: Vac. Surfaces Films* **1996**, *14*, 631.
[251] M. Rosenberg, *J. Plasma Phys.* **2002**, *67*, 235.
[252] A. Piel, M. Klindworth, O. Arp, A. Melzer, M. Wolter, *Phys. Rev. Lett.* **2006**, *97*, 205009.
[253] A. Piel, M. Klindworth, O. Arp, A. Melzer, M. Wolter, *Phys. Rev. Lett.* **2007**, *99*, 209903.
[254] V. V. Yaroshenko, *Phys. Rev. E* **2020**, *102*, 023201.
[255] S. Khrapak, V. Yaroshenko, *Plasma Phys. Control. Fusion* **2020**, *62*(10), 105006.
[256] K. Quest, M. Rosenberg, A. Levine, *J. Plasma Phys.* **2020**, *86*, 905860605.
[257] N. N. Rao, P. K. Shukla, M. Y. Yu, *Planet. Space Sci.* **1990**, *38*, 543.
[258] M. A. Fink, S. K. Zhdanov, M. Schwabe, M. H. Thoma, H. Höfner, H. M. Thomas, G. E. Morfill, *Europhys. Lett.* **2013**, *102*, 45001.
[259] A. Piel, *AIP Conf. Proc.* **2011**, *1397*(1), 50.
[260] M. Schwabe, S. A. Khrapak, S. K. Zhdanov, M. Y. Pustylnik, C. Räth, M. Fink, M. Kretschmer, A. M. Lipaev, V. I. Molotkov, A. S. Schmitz, M. H. Thoma, A. D. Usachev, A. V. Zobnin, G. I. Padalka, V. E. Fortov, O. F. Petrov, H. M. Thomas, *New J. Phys.* **2020**, *22*, 083079.
[261] D. Cheng-Ran, H. M. Thomas, A. V. Ivlev, U. Konopka, G. E. Morfill, *Phys. Plasmas* **2010**, *17*(11), 113710.
[262] S. Dap, D. Lacroix, R. Hugon, L. de Poucques, J.-L. Briancon, J. Bougdira, *Phys. Rev. Lett.* **2012**, *109*, 245002.
[263] B. Tadsen, F. Greiner, S. Groth, A. Piel, *Phys. Plasmas* **2015**, *22*(11), 113701.
[264] B. Tadsen, F. Greiner, A. Piel, *Phys. Rev. E* **2018**, *97*, 033203.
[265] S. Arndt, F. Sigeneger, H. Testrich, C. Brandt, *Plasma Chem. Plasma Process.* **2005**, *25*, 567.
[266] A. V. Zobnin, A. D. Usachev, O. F. Petrov, V. E. Fortov, *Phys. Plasmas* **2015**, *22*, 094702.
[267] J. L. Dorier, C. Hollenstein, A. A. Howling, *J. Vac. Sci. Technol. A* **1995**, *13*, 918.
[268] G. E. Morfill, H. M. Thomas, U. Konopka, H. Rothermel, M. Zuzic, A. Ivlev, J. Goree, *Phys. Rev. Lett.* **1999**, *83*, 1598.
[269] V. V. Balabanov, L. M. Vasilyak, S. P. Vetchinin, A. P. Nefedov, D. N. Polyakov, V. E. Fortov, *J. Exp. Theor. Phys.* **2001**, *92*(1), 86.
[270] L. M. Vasilyak, S. P. Vetchinin, D. N. Polyakov, V. E. Fortov, *J. Exp. Theor. Phys.* **2005**, *100*, 1029.
[271] A. V. Fedoseev, G. I. Sukhinin, A. R. Abdirakhmanov, M. K. Dosbolayev, T. S. Ramazanov, *Contributions Plasma Phys.* **2016**, *56*, 234.
[272] H. Totsuji, *Plasma Phys. Control. Fusion* **2016**, *58*, 045010.
[273] D. N. Polyakov, V. V. Shumova, L. M. Vasilyak, *Plasma Sources Sci. Technol.* **2017**, *26*, 08LT01.
[274] V. V. Shumova, D. N. Polyakov, L. M. Vasilyak, *Plasma Phys. Rep.* **2019**, *45*, 285.
[275] V. V. Shumova, D. N. Polyakov, E. K. Mataybaeva, L. M. Vasilyak, *Phys. Lett. A* **2019**, *383*, 125853.
[276] V. V. Shumova, D. N. Polyakov, L. M. Vasilyak, *Russ. J. Phys. Chem. B* **2020**, *14*, 666.
[277] W. J. Goedheer, V. Land, J. Venema, *Contributions Plasma Phys.* **2009**, *49*, 199.
[278] C. Schmidt, O. Arp, A. Piel, *Phys. Plasmas* **2011**, *18*(1), 013704.
[279] I. Pilch, F. Greiner, *J. Appl. Phys.* **2017**, *121*(11), 113302.
[280] K. Avinash, *Phys. Plasmas* **2001**, *8*, 2601.
[281] R. P. Dahiya, G. V. Paeva, W. W. Stoffels, E. Stoffels, G. M. W. Kroesen, K. Avinash, A. Bhattacharjee, *Phys. Rev. Lett.* **2002**, *89*, 125001.
[282] M. Wolter, A. Melzer, O. Arp, M. Klindworth, A. Piel, *Phys. Plasmas* **2007**, *14*(12), 123707.
[283] M. Kretschmer, S. A. Khrapak, S. K. Zhdanov, H. M. Thomas, G. E. Morfill, V. E. Fortov, A. M. Lipaev, V. I. Molotkov, A. I. Ivanov, M. V. Turin, *Phys. Rev. E* **2005**, *71*, 056401.
[284] E. Thomas, B. M. Annaratone, G. E. Morfill, H. Rothermel, *Phys. Rev. E* **2002**, *66*, 016405.
[285] B. Buttenschön, M. Himpel, A. Melzer, *New J. Phys.* **2011**, *13*, 023042.
[286] M. Kretschmer, U. Konopka, S. K. Zhdanov, H. M. Thomas, G. E. Morfill, V. E. Fortov, V. I. Molotkov, A. M. Lipaev, O. F. Petrov, *IEEE Trans. Plasma Sci.* **2011**, *39*(11), 2758.
[287] J. Goree, G. E. Morfill, V. N. Tsytovich, S. V. Vladimirov, *Phys. Rev. E* **1999**, *59*, 7055.
[288] V. N. Tsytovich, S. V. Vladimirov, G. E. Morfill, J. Goree, *Phys. Rev. E* **2001**, *63*, 056609.
[289] V. N. Tsytovich, S. V. Vladimirov, G. E. Morfill, *Phys. Rev. E* **2004**, *70*, 066408.
[290] G. Morfill, V. N. Tsytovich, *Plasma Phys. Rep.* **2000**, *26*, 682.
[291] K. Avinash, A. Bhattacharjee, S. Hu, *Phys. Rev. Lett.* **2003**, *90*, 075001.
[292] Y. Liu, S. Mao, Z.-X. Wang, X. Wang, *Phys. Plasmas* **2006**, *13*, 064502.
[293] C. S. Ng, A. Bhattacharjee, S. Hu, Z. W. Ma, K. Avinash, *Plasma Phys. Control. Fusion* **2007**, *49*, 1583.
[294] D. Samsonov, J. Goree, *IEEE Trans. Plasma Sci.* **1999**, *27*(1), 76.
[295] M. Mikikian, S. Labidi, E. von Wahl, J.-F. Lagrange, T. Lecas, V. Massereau-Guilbaud, I. Géraud-Grenier, E. Kovacevic, J. Berndt, H. Kersten, T. Gibert, *AIP Conf. Proc.* **2018**, *1925*(1), 020019.
[296] J. Goree, R. Quinn, G. Morfill, H. Thomas, T. Hagl, U. Konopka, H. Rothermel, M. Zuzic, *Proc. 4th Microgravity Fluid Phys. Transp. Phenom. Conf*., Cleveland, **1998**, 105–106. https://ntrs.nasa.gov/citations/20010006305.
[297] S. K. Zhdanov, M. Schwabe, R. Heidemann, R. Sütterlin, H. M. Thomas, M. Rubin-Zuzic, H. Rothermel, T. Hagl, A. V. Ivlev, G. E. Morfill, V. I. Molotkov, A. M. Lipaev, O. F. Petrov, V. E. Fortov, T. Reiter, *New J. Phys* **2010**, *12*, 043006.
[298] M. Mikikian, L. Boufendi, *Phys. Plasmas* **2004**, *11*, 3733.

[299] M. Mikikian, L. Couëdel, M. Cavarroc, Y. Tessier, L. Boufendi, *New J. Phys.* **2007**, *9*, 268.
[300] M. Mikikian, M. Cavarroc, L. Couëdel, Y. Tessier, L. Boufendi, *Phys. Rev. Lett.* **2008**, *100*, 225005.
[301] M. Mikikian, L. Couëdel, M. Cavarroc, Y. Tessier, L. Boufendi, *Phys. Rev. Lett.* **2010**, *105*, 075002.
[302] Aleksandr Pikalev, Mikhail Pustylnik, Christoph Räth, Hubertus Thomas, Submitted to Phys. Rev. E, **2021**.
[303] M. Mikikian, M. Cavarroc, N. Chaumeix, L. Boufendi, 31st EPS Conf. Plasma Phys. London, 28 June-July 2, 2004, London, 28G *ECA*, **2004**, O–2.13. http://epsppd.epfl.ch/London/pdf/O2_13.pdf.
[304] M. Schwabe, S. Zhdanov, C. Räth, *IEEE Trans. Plasma Sci.* **2018**, *46*, 684.
[305] S. V. Vladimirov, V. N. Tsytovich, G. E. Morfill, *Phys. Plasmas* **2005**, *12*, 052117.

How to cite this article: M. Pustylnik, A. Pikalev, A. Zobnin, I. Semenov, H. Thomas, O. Petrov, *Contributions to Plasma Physics* **2021**, e202100126. https://doi.org/10.1002/ctpp.202100126